



RESEARCH ARTICLE OPEN ACCESS

CD147 Mediates the Metabolic Reprogramming of Cancer Associated Fibroblasts Induced by EVs Released by Differentiating Cancer Stem Cells

Filomena Colella¹ | Federica Calapà² | Giulia Artemi³ | Erica Pazzaglia³ | Rita Colonna³ | Sara Vitale² | Giacomo Lazzarino⁴ | Federica Vincenzoni⁵ | Micol Eleonora Fiori²  | Ruggero De Maria^{1,3} | Sara Lucchisani² | Giannicola Genovese⁶ | Luigi Perelli⁶ | Barbara Tavazzi⁴ | Alessandro Sgambato^{1,3}  | Donatella Lucchetti^{1,3}

¹Multiplex Spatial Profiling Facility, Fondazione Policlinico Universitario 'Agostino Gemelli' IRCCS, Rome, Italy | ²Department of Oncology and Molecular Medicine, Istituto Superiore di Sanità, Rome, Italy | ³Department of Translational Medicine and Surgery, Università Cattolica del Sacro Cuore, Rome, Italy | ⁴UniCamillus - Saint Camillus International University of Health and Medical Sciences, Rome, Italy | ⁵Dipartimento di Scienze Biotecnologiche di Base, Cliniche Intensivologiche e Perioperatorie, Università Cattolica del Sacro Cuore, Rome, Italy | ⁶Department of Genitourinary Medical Oncology, The University of Texas MD Anderson Cancer Center, Houston, USA

Correspondence: Alessandro Sgambato (alessandro.sgambato@unicatt.it)

Received: 19 August 2024 | **Revised:** 24 January 2025 | **Accepted:** 31 January 2025

Keywords: cancer-associated fibroblasts | CD147 | extracellular vesicles | tumour microenvironment

ABSTRACT

Several reports have demonstrated that CD147, an N-glycosylated protein that is exchanged by cells in soluble form or through small extracellular vesicles (sEVs), can promote cancer progression. However, its activity related to EVs in colorectal cancer (CRC) is still not fully understood. Previously, we showed that sEV secretion during CRC stem cell (CR-CSCs) differentiation is partially controlled by CD147, and that CD147-expressing sEVs (sEVs-CD147) activate a signalling cascade in recipient cells, inducing molecular invasive features in CR-CSCs. In the present study, we demonstrated that sEVs-CD147 increase the expression of myofibroblast and activation markers in cancer-associated fibroblasts (CAF). In sEVs-CD147-activated CAF, aerobic glycolysis was also triggered by the β -catenin signalling pathway and induced lactate release. These effects were associated with NFKB upregulation and NO secretion that caused increased cytokines production and VEGF release, respectively. Furthermore, co-culture with CAF promoted CR-CSC invasivity in vitro and tumour growth in vivo. Spatial proteomics analysis confirmed in vivo the activation of fibroblasts and the modulation of their metabolic features, within their biological context, after their conditioning with CD147-expressing sEVs. Our findings indicate that sEV-packaged CD147 is involved in CAF activation, thus promoting tumour progression via stroma metabolism modification.

1 | Introduction

Colorectal cancer (CRC) is the third most common type of cancer and the second most common cause of cancer deaths worldwide leading to almost 1 million deaths per year (Sung

et al. 2021). Several pieces of evidence have shown that tumour progression might not only rely on the cancer cells themselves but also be influenced by the tumour microenvironment (TME) (Greaves and Maley 2012). Among surrounding stroma cells, cancer-associated fibroblasts (CAF) are characterized by the

Abbreviations: CAF, cancer-associated fibroblasts; CRC, colorectal cancer; CR-CSCs, colorectal cancer stem cells; CSCs, cancer stem cells; FAP, fibroblast activation protein; MMPs, matrix metalloproteinases; MVs, multivesicular bodies; NFs, normal fibroblasts; sEVs, small extracellular vesicles; VIM, vimentin; α -SMA, α -smooth muscle actin.

This is an open access article under the terms of the [Creative Commons Attribution-NonCommercial-NoDerivs](https://creativecommons.org/licenses/by-nc-nd/4.0/) License, which permits use and distribution in any medium, provided the original work is properly cited, the use is non-commercial and no modifications or adaptations are made.

© 2025 The Author(s). *Journal of Extracellular Biology* published by Wiley Periodicals, LLC on behalf of the International Society for Extracellular Vesicles.

expression of α -smooth muscle actin (α -SMA), vimentin (VIM) and fibroblast activation protein (FAP) (Li et al. 2021). They are mainly derived from normal fibroblasts (NFs) in the surrounding tissue. Several intracellular signalling pathways, such as NF- κ B, ERK and AKT, have been reported to regulate the reprogramming of CAF, thereby creating a microenvironment that contributes to promoting cancer growth, invasiveness, metastasis and resistance to therapy (Kalluri 2016). The crosstalk between CRC cells and CAF has been studied extensively. However, the specific mechanisms of fibroblast activation by cancer cells remain unclear in CRC. Small extracellular vesicles (sEVs) are vesicles that originate from multivesicular bodies (MVBs) and are secreted when these compartments fuse with the plasma membrane (Lucchetti et al. 2020). They mediate cell-to-cell communication and activate signalling pathways in recipient cells through their cargo of proteins, nucleic acids, and lipids (Lucchetti et al. 2017, Lucchetti et al. 2020). Recently, it has been shown that EVs are involved in the metabolic switch occurring in cancer and tumour-stroma cells (fibroblasts, endothelial and immune cells) (Yan et al. 2018, Patel et al. 2019). Several pieces of evidence suggest that CAF can secrete metabolites to sustain the growth of tumour cells (Yan et al. 2018, Patel et al. 2019). When fibroblasts are co-cultured with cancer cells, they are forced to undergo aerobic glycolysis and produce energy-rich nutrients (such as lactate) to “feed” cancer cells, a phenomenon known as “Reverse Warburg Effect” (Lucchetti et al. 2020). CD147, termed basigin in mice and also known as EMMPRIN, is a type I transmembrane glycoprotein overexpressed in various types of cancer tissues (Nyalali et al. 2023). The best-known function of CD147 relevant to tumorigenesis is to induce the production of various matrix metalloproteinases (MMPs) in cancer cells and fibroblasts through epithelial–stromal interaction, leading to degradation of extracellular matrix, thus facilitating cancer cell invasion and metastasis (Luo et al. 2014). CD147 overexpression correlates with poor prognosis in several types of solid tumours, including colon cancer (Nyalali et al. 2023). Moreover, Xu and colleagues demonstrated that CD147 has a role in transforming fibroblasts to CAF in breast cancer by mediating the induction of α -SMA (Xu et al. 2013). Aoki et al. showed that CD147 can stimulate fibroblasts increasing the secretion of MMP2 and promoting invasion (Aoki et al. 2019). Several reports have demonstrated that CD147 transferred in soluble form or by sEVs, can promote cancer progression (Lucchetti et al. 2020). However, its activity is still not fully understood. Previously, we showed that sEVs secretion during CR-CSC differentiation is partially controlled by CD147, and that CD147-expressing sEVs (sEVs-CD147) activate a signalling cascade in recipient cells, inducing molecular invasive features (Lucchetti et al. 2020). So far, no study has investigated the role of sEVs-CD147 in CAF metabolism and how differentiation impacts its function.

2 | Materials and Methods

2.1 | Cell Culture

CR-CSC lines (CSC1 and CSC2) were isolated as previously described (Lucchetti et al. 2020) and were maintained onto T175 low-attachment plates in serum-free medium (basal culture medium) supplemented with 20 ng/mL epidermal growth factor (EGF) and 10 ng/mL FGF-2 (Pepro Tech, Rocky Hill, NY, USA).

It is noteworthy that, as previously reported, the CSC1 and CSC2 cells used for the study have different genetic backgrounds, being KRAS and BRAF mutated, respectively, thus resembling the genetic variability of CRC in vivo (Lucchetti et al. 2020). Differentiation was induced by culturing 2.5×10^6 CR-CSCs with 15 mL of medium supplemented with 10% FBS (foetal bovine serum) in the absence of growth factors for 8 days. When cells reached the differentiation condition (80% of confluency), the medium was replaced with basal culture medium supplemented with 2 mM NaB or an equal volume of vehicle (PBS). After 48 h, media were collected for EV isolation. Human colon-derived fibroblasts were isolated from freshly resected operative specimens from patients undergoing surgery for primary, previously untreated CRC at the Division of Surgery, Fondazione Policlinico Agostino Gemelli (Rome, Italy). CAF were isolated from the tumour mass while normal non-cancer-associated fibroblasts (NFs) were isolated from adjacent normal mucosa. Both cancer and non-tumorigenic specimens were washed two times with PBS, then minced into approximately 1–2 mm² sized pieces and digested using 5 mL of a lysis buffer (150 mmol/L NH₄Cl, 100 mmol/L KHCO₃, 10 mmol/L EDTA pH 8) with 0.75 μ g/ μ L collagenase I (Sigma Chemical Co., St. Louis, MO, USA). After 40 min, the homogenate was collected and passed through a 70 mmol/L strainer. CAF and NFs were then resuspended and plated in Dulbecco’s modified Eagle’s medium F12 medium, 1% penicillin/streptomycin, 10% FBS (Gibco), 0.1% gentamicin, 1% amphotericin B, and 1% sodium pyruvate. After 24 h of culture, the medium was replaced to eliminate floating cells.

2.2 | Purification and Characterization of sEVs

Conditioned cell culture media enriched in sEVs were centrifuged at $750 \times g$ for 15 min and then at $1500 \times g$ for 5 min. Supernatants were saved and centrifuged at $17,000 \times g$ for 45 min. The pellets composed of extracellular vesicles (EVs) were washed in PBS by centrifugation at $17,000 \times g$ for 45 min. Supernatants were transferred to fresh tubes and centrifuged at $120,000 \times g$ for sEV purification. sEV pellets were resuspended in PBS and used for further characterization (see next sections) and for the treatment of cells or to prepare protein extracts for Western blot analysis. The Bradford assay was used for the quantitative evaluation of sEVs.

2.3 | Nanoparticle Tracking Analysis (NTA)

The size and concentration profiles of small EVs were determined using a Nanosight NS300 instrument (Malvern), and analysed by NTA software version 3.4, build 3.4.4. Silica microspheres of 100 nm were routinely analysed to verify the instrument’s performance. EVs were prepared for NTA analysis by diluting 1:50–1:100 in 1 mL of PBS. EV preparations were loaded into the sample chamber and analysed following the measurement script: initial; 5-s delay; 30-s acquisition; measurements were repeated 5 times per sample. The camera gain was set to level 15 for all measurements. Acquisitions were analysed using proprietary software.

2.4 | Transmission Electron Microscopy

For transmission electron microscopy, sEVs were fixed and stained with a solution of 5% uranyl acetate and 50% ethyl alcohol in water. Samples were loaded on a copper grid and incubated

for 30–60". After rinses, samples are observed using Zeiss Libra 120 (Zeiss NTS GmbH, Oberkochen, Germany), as previously reported (Lucchetti et al. 2020).

2.5 | SDS-PAGE and RP-UHPLC-High Resolution MS/MS Characterization of Tryptic Peptides

Sodium dodecyl sulphate poly acrylamide gel electrophoresis (SDS-PAGE) separation was performed by loading an aliquot (15 µg) of sEV extracts on 12% Bis Tris Criterion XT precast gel (Bio-Rad Laboratories, Inc. United States). The gel lanes resulting from each sample (analysed in duplicate) were cut into slices and subjected to in gel digestion protocol (Shevchenko et al. 2006). Tryptic peptides were lyophilized and resuspended with 15 µL of 0.1% FA solution for mass spectrometry analysis. Proteomic characterizations were carried out by an UHPLC UltiMate 3000 RSLCnano System coupled to Orbitrap Elite MS detector with EASY-Spray nano ESI source (Thermo Fisher Scientific, Waltham, MA, USA). Chromatographic separations were performed at 35°C on a PepMap C18 EASY-Spray column 15 cm in length × 50 µm of internal diameter (ID) (2 µm particles, 100 Å pore size), in coupling with Acclaim PepMap100 nano-trap cartridge (C18, 5 µm, 100 Å, 300 µm, id 5 mm) (Thermo Fisher Scientific), using aqueous solution of formic acid (FA 0.1%, v/v) as Eluent A and acetonitrile/water/FA solution (ACN/FA 99.9:0.1, v/v) as Eluent B. The gradient elution was 0–7 min 3% B, 7–35 min from 3 to 55% B (linear), 35–36 min from 55 to 90% B (linear), at a flow rate of 0.3 µL/min with a total run of 60 min. The injection volume was 5 µL. Full MS spectra were recorded in positive ionization mode over a 300–2000 m/z acquisition range and with a 60,000-scan resolution. Each full scan was followed by MS/MS events of the five most intense signals acquired in the linear ion trap at normal scan rate during the data dependent scan (DDS) mode, selected with an isolation width to 2 m/z and fragmented by collision-induced dissociation (CID) with normalized collision energy of 35%. The data analysis was performed by Proteome Discoverer 1.4 software (version 1.4.1.14, Thermo Fisher Scientific). Proteins identified stringent filters criteria according to Human Proteome Project Organization (HUPO) filters, were analysed by FunRich software, a stand-alone software tool, used mainly for functional enrichment and interaction network analysis of genes and proteins. The PANTHER database was used to identify the related metabolic pathways.

2.6 | Sample Preparation and Chromatographic Conditions of the HPLC Analysis of Low Molecular Weight Metabolites

The targeted metabolomics analyses were performed after the deproteinization of cell samples (1×10^6 cells) according to a protocol suitable for obtaining protein-free extracts suitable for the subsequent HPLC analysis of acid labile and easily oxidizable compounds (Lazzarino et al. 2003; Yakoub et al. 2019). Cell cultures were washed twice in ice-cold PBS and subsequently centrifuged at $1890 \times g$ for 10 min at 4°C, producing a cell pellet and a supernatant. Cell pellets were deproteinized with the addition of 1 mL of ice-cold, nitrogen-saturated, 10 mM pH 7.4 KH_2PO_4 in CH_3CN (1:3, v/v). After vigorous vortexing for 60 s, the samples were centrifuged at $20,690 \times g$ for 15 min at 4°C. The protein-free supernatants were collected and subjected to 2 chloroform

washings, to eliminate the organic solvent and obtain an upper aqueous phase that was directly injected onto the HPLC. The simultaneous separation and quantification of low-molecular weight metabolites related to energy metabolism, antioxidants and indexes of post-translational N-linked glycosylation of proteins and of RNA turnover, including high energy phosphates (ATP, ADP), oxidized and reduced nicotinic coenzymes (NAD^+ , NADH, NADP^+ , and NADPH), glycosylated UDP-derivatives (UDP-galactose, UDP-glucose), β -pseudouridine and reduced glutathione (GSH) were performed in each sample of cell extracts, according to an ion pairing HPLC method previously set up in our laboratories (Lazzarino et al. 2003; Yakoub et al. 2019). The HPLC apparatus consisted of a Surveyor HPLC system (ThermoFisher Italia, Rodano, Milan, Italy), equipped with a 5-cm light-path flow cell, set up between 200 and 400 nm wavelength for acquisition of chromatographic runs. Data acquisition and analysis were performed using the ChromQuest software package (5.0 version) provided by the HPLC manufacturer. Separation of the various compounds was carried out using a Hypersil 250 × 4.6 mm, 5 µm particle-size column, which was provided with its own guard column (Thermo Fisher Scientific, Rodano, Milan, Italy). Species identification and quantification in deproteinized samples of cell extracts were done by matching retention times, peak areas and absorption spectra of those of freshly prepared ultrapure standards. The concentrations of metabolites of interest were determined at 260 nm wavelength, except for GSH, whose concentrations were determined at 206 nm. In cell extracts, the total amount of proteins was determined according to the Bradford method (Bradford 1976). All concentration values of metabolites of interest were normalized for the total cell protein content and expressed as nmol/mg of proteins.

2.7 | Determination of Lactate Levels in Extracellular Medium

The spectrophotometric determination of lactate was carried out on extracellular culture media using an Agilent 89090A spectrophotometer (Agilent Technologies, Santa Clara, CA, USA), following the method described by Artiss et al. (2000), as reported in detail (Amorini et al. 2014). Briefly, the reaction mixture contained 100 mM Tris-HCl, 1.5 mM N-ethyl-N-2-hydroxy-3-sulfopropyl-3-methylalanine, 1.7 mM 4-aminoantipyrine, and 5 IU horseradish peroxidase. Fifty microliters of extracellular medium were added to the mixture, left to stand for 5 min and read at 545 nm wavelength. The reaction was started with the addition of 5 IU of lactate oxidase to the cuvette (finale volume = 1 mL) and it was considered ended when stable absorbance readings were obtained. To calculate lactate concentration in extracellular medium samples, the difference in absorbance at 545 nm wavelength (Δabs) of each sample was interpolated with a calibration curve obtained by plotting Δabs measured in solutions of standard lactate with increasing known concentrations. Extracellular lactate concentrations were normalized for the total cell protein content and expressed as nmol/mg of proteins.

2.8 | In Vivo Study

All animal experiments were approved by the institutional animal care and use committees at ISS (n°1157/2020-PR). For in vivo studies, CAF were cultured for 72 h with or without EVs. On

Day 3, CR-CSCs were dissociated as described above (Lucchetti et al. 2020), and resuspended in 50% PBS / 50% Matrigel Basement Membrane Matrix (BD Biosciences, Franklin Lakes, New Jersey, USA). CSCs alone (5×10^5 cells/mouse) or mixed with CAF (1.5×10^6 cells/mouse) were injected subcutaneously in the flank of NSG mice ($n = 6$). On Days 7, 14, and 21, mice were treated peritumorally with vehicle or EVs (3×10^8 particles/mL). Moreover, EVs were added to CRC-SCs medium on Days 1 and 4. After 7 days of culture CRC-SCs were dissociated, resuspended in 50% PBS/50% Matrigel and injected subcutaneously (5×10^5 cells/mouse) in the flank of NSG mice ($n = 6$).

Xenografts were measured once a week by digital calliper, and volumes were calculated using the following formula: $\pi/6 \times d^2 \times D$, where d and D represent shorter and longer tumour measurements, respectively. Mice were sacrificed 5 weeks after cell injection, and xenografts were harvested and formalin-fixed paraffin-embedded for subsequent analyses.

2.9 | Tube Formation Assays

Matrigel Basement Membrane Matrix (BD Biosciences) was diluted at a concentration 3 mg/mL and 50 μ L/cm² was added to a 24-well plate. Then gel was allowed to polymerize at 37°C for 60 min. After Matrigel polymerization, HUVECs cell suspension (3×10^4 cells/well) was added onto the solidified matrix gel supplemented with sEVs or with VEGF (20 ng/mL, positive control). Tube formation was observed under an inverted microscope (Zeiss Axiovert 40 CFL) after 24 h. Images were captured with a Zeiss AxioCam camera attached to the microscope. The tube formation was quantified by measuring the long axis of the individual cells on the matrix using the Image J Angiogenesis Analyzer. Mean values of branch points and total length in each sample were used to numerically represent tube formation.

2.10 | Luminex Assay

CD147, IL8, and IL6 concentrations were determined in conditioned media using a Luminex assay (multiplex biometric ELISA-based immunoassay) and run on a Luminex 200 System (Luminex Corporation, Austin, TX) according to the manufacturer's instructions. Results were analysed using a dedicated Bio-Plex Manager software. The medium was obtained from 15×10^3 CAF treated for 48 h with EV, respectively: (I) CAF without sEVs; (II) CAF + sEVs, CAF treated with sEVs isolated from CR-CSC and having a low expression of CD147 (3×10^8 particles/mL); (III) CAF + sEVs N-gly CAF treated with sEVs pretreated with N-glycosidase F (15 mU/mL) for 30 min at 37°C, isolated from CR-CSC and having a low expression of CD147 (3×10^8 particles/mL); (IV) CAF + sEVs Ab CAF treated with sEVs pretreated with anti-CD147 Antibody (1.5 μ g of antibody for 3×10^8 particles/mL) for 2 h at 4°C, isolated from CSC and having a low expression of CD147.

2.11 | Invasion Assay

Colon cancer HT29 and CR-CSC cells were seeded onto the upper chamber of each Transwell insert at a density of 5×10^4 cells of 96 well plate Corning FluoroBlok. The invasion chambers were

then incubated for 48 h at 37°C to allow for cell invasion through the Matrigel-coated membrane towards the chemoattractants in the lower chamber. Matrigel was thawed on ice and diluted with ice-cold serum-free DMEM to a final concentration of 3 mg/mL. The diluted Matrigel was added to the upper surface of each Transwell insert. Chambers were then incubated at 37°C for 2 h to allow Matrigel solidification. The lower chamber was filled with different medium conditions to serve as chemoattractants for cell invasion. The following medium conditions were used: (I) NT: Fresh DMEM/F12 medium, 1% glutamine, and 1% penicillin-streptomycin (Pen/Strep) for HT29 and fresh NCS medium for CR-CSC. (II) CTR: conditioned medium for 48 h by CAF; (III) CAF + sEVs-CD147 low: conditioned medium for 48 h by CAF, treated with sEVs isolated from CR-CSC and having a low expression of CD147; (IV) CAF + sEVs-CD147 medium: conditioned medium for 48 h by CAF treated with sEVs isolated from differentiated CR-CSC having a medium expression of CD147; (VI) CAF + sEVs-CD147 high: conditioned medium for 48 h by CAF, treated with sEVs isolated from NAB differentiated CR-CSC. To assess cell invasion, the invaded cells on the lower side of the membrane were stained with green calcein with 1 μ M calcein AM (Life Technologies) in serum-free DMEM for 30 min at 37°C in the dark. Fluorescent images of invaded cells were captured using a Nikon fluorescence microscope (Nikon) equipped with a FITC channel.

2.12 | Immunofluorescence Staining

For co-culture assay, a density of 1×10^6 cells/mL of HT29 cells were seeded to the Transwell inserts sides in a 24 wells plate with a 15 mm diameter cover glass on bottom. After 24 h, the inserts were removed and 15×10^3 CAF were pretreated for 48 h with EV, respectively (I) NT: without sEVs; (II) CTR: sEVs-CD147 low (3×10^8 particles/mL); (III) sEVs-CD147 high (3×10^8 particles/mL), were incubated for 25 h with HT29. For EVs uptake assay, 2×10^4 cells were grown in 8-well culture slides and were incubated with EVs (3×10^8 particles/mL) marked with PE anti-human CD9 antibody (312105, Biolegend, San Diego, CA, USA) for 10', 30', 1 h. Then, the cells were fixed with 4% paraformaldehyde for 30 min and permeabilized with triton X-100 (0.1% in PBS) for 10 min and blocked with 3% normal goat serum/PBS for 30 min at room temperature. Then, cells were incubated with primary antibody monoclonal anti-mouse Alpha-Smooth Muscle ((1A4), code 14-9760-82, Thermo Fisher Scientific, dilution 1:200) and monoclonal anti-rabbit Keratin 20 ((D9Z1Z), 13063, Cell Signaling Technology, dilution 1:400) overnight at 4°C, followed by incubation with secondary antibody Alexa 488 donkey anti-rabbit IgG (1:1000, Thermo Fisher Scientific, Cat# A-21206) and Alexa Fluor 633 goat anti-mouse IgG secondary antibody (1:5000; Thermo Fisher Scientific, Cat# A-21052). Subsequently, the slides were mounted with DAPI (Fluoromount G with DAPI; Electron Microscopy Sciences, Hatfield, PA, USA). The images (40 \times) were acquired with Vectra Polaris Automated Quantitative Pathology Imaging System (Akoya Biosciences) and the analysis was performed with Image J (NIH, Bethesda, MA, USA).

2.13 | Multiplex IHC

Tumours were excised from mice, formalin-fixed and paraffin-embedded and sectioned at 5 μ m. The Opal 6-color IHC kit (PerkinElmer, Waltham, USA, Cat. No. NEL820001KT) was used

for the multiplex immunolabeling by automated immunostainer, Leica BOND RX (Leica Microsystems, Milton Keynes, UK). Detailed information on the antibodies, including their dilutions and retrieval buffers, is given below. Fluorophores and DAPI were prepared according to the manufacturer's guidelines. The slides were processed at 20× magnification and acquired using the Vectra Polaris Automated Quantitative Pathology Imaging System (Akoya Biosciences), and analysis was performed using Akoya Bioscience's inForm software. All data processing and visualisation procedures were performed using R (version 4.2.2), facilitated by the phenoptrReports and phenoptr packages.

2.15 | Western Blot Analysis

Cells or sEVs pellet were lysed using lysis buffer (50 mmol/L Tris-HCl pH 7.2, 5 mmol/L MgCl₂, 50 mmol/L NaCl, 0.25%, 0.1% SDS, and 1% Triton X-100) containing protease inhibitors (2 mmol/L phenyl methyl sulfonyl fluoride, 10 mg/mL aprotinin, and 2 mmol/L Na₃VO₄, 100 mmol/L NaF). To separate cytoplasmic, membrane, and nuclear soluble proteins, cells were lysed using the Subcellular Protein Fraction kit for Cultured Cells (Thermo Fisher Scientific, Waltham, MA, USA). Protein concentration was determined by the Bradford method (Bradford protein assay kit II,

Order	Antibody	Supplier	Clone	Catalogue	Dilution factor	Opal pairing	Retrieval and incubation time
1	MCT4	Santa Cruz	(D-1)	sc-376140	1:200	690	ER1 30'
2	CD147	abcam	EPR4053	ab108308	1:250	520	ER1 30'
3	MCT1	Bethyl Laboratories	polyclonal	A304-398a-M	1:200	570	ER1 30'
4	PANCK	Cell Signaling Technology	AE1 AE3	67306	1:100	480	ER2 45'
5	FAP	Thermo Fisher Scientific	polyclonal	PA5-120990	1:900	620	ER1 30'
6	Alpha sma	Thermo Fisher Scientific	(1A4)	14-9760-82	1:200	780	ER1 30'

2.14 | RT-qPCR Assays

Total RNA was extracted from cells and sEVs using the RiboPure™ RNA Purification Kit (Ambio, Thermo Fisher Scientific UK Ltd.) and cDNA was prepared using the iScript cDNA Synthesis Kit (Bio-Rad Laboratories S.r.l., Segrate, Milan, Italy). Each real-time polymerase chain reaction (PCR) was performed in triplicate using SSOADV-univer-SYBR-GREEN (Bio-Rad Laboratories S.r.l., Segrate, Milan, Italy). Analysis was performed using the CFX96 Touch Real-Time PCR Detection System (Bio-Rad Laboratories S.r.l.), and acquisition and data processing were performed using CFX Manager software version 1.6 (Bio-Rad Laboratories S.r.l.). Primer sequences are reported in the table below.

Bio-Rad, Hercules, CA, USA), with BSA as a standard. The protein extracted from cell lysates (40 µg) and EVs (10 µg) were resolved by SDS-PAGE 10% under reducing or non-reducing conditions and were transferred to PVDF blotting membranes (GE Healthcare, Solingen, Germany). Analysis was performed using the enhanced chemiluminescence kit for Western blotting detection (Advansta, WesternBright™ ECL, Bering Drive San Jose, CA, USA). The primary monoclonal antibodies used are listed in the table below.

	Forward	Reverse
HK2	TGCCACCAGACTAACTAGACG	CCCGTGCCCAATGAGAC
SLC2A1	GGCCAAGAGTGTGCTAAAGAA	CCTTCTTCTCCCGCATCATCTG
SLC16A3	CGGCTTTGTGCTTTACGCC	GCTGAAGAGGTAGACGGAGTA
PMG2	GAGCTGCTATGGGACCTGGA	GCTCGGGCGTCAAACTGA
PKM	ATTATTTGAGGAACTCCGCCGCCT	ATTCCGGGTCACAGCAATGATGG
ENO2	CCGGGAACCTCAGACCTCATC	CTCTGCACCTAGTCGCATGG
ME1	GGGAGACCTTGCTGTAATGG	TTCGGTTCCACATCCAGAAT
G6PD	ACCGCATCGACCACTACCT	TGGGGCCGAAGATCCTGTT

Antibody	Code	Vendor	Dilution
β -Actina	sc-47778	Santa Cruz	1:1000
CD147	sc-21746	Santa Cruz	1:500
UGP2	sc-377089A	Santa Cruz	1:500
PKM2	sc-365684	Santa Cruz	1:100
VIMENTIN	GTX112661	GeneTex	1:500
Alpha sma	14-9760-82	Thermo Fisher Scientific	1:200
FAP	PA5-120990	Thermo Fisher Scientific	1:500
GAPDH	sc-47724	Santa Cruz	1:1000
MCT4	A304-398a-M	Bethyl Laboratories	1:200
NFK β	sc 372	Santa Cruz	1:200
VEGF	sc-7269	Santa Cruz	1:500
E-Cadherin	3195	Cell Signaling	1:1000
NEU1	sc-16682	Santa Cruz	1:500
EGFR	Sc-373746	Santa Cruz	1:500

3 | Results

3.1 | CR-CSC-Released sEVs Are Internalized by CAF and NFs and Their Effect Correlates With CD147 Expression Level

We previously showed that, during differentiation of CR-CSCs, CD147 expression increases in sEVs compared to sEVs released by control undifferentiated cells (7). In this study, we investigated the effects of CR-CSC-derived sEVs on fibroblasts activation and whether they are affected by the differentiation of the releasing cells. Moreover, we aimed to evaluate whether CD147 play a role in such effects. To this aim, we isolated and purified sEVs from conditioned medium of two CR-CSC lines (CR-CSC-1; CR-CSC-2) (isolated from surgical specimens of CRC patients), differentiated by two different strategies: (1) replacing growth factors with 10% FBS in the culture medium (see Materials and Methods section for details) and growing cells up to confluence; (2) growing cells as in (1) for 1 week and then adding 2 mM of sodium butyrate (NaB, differentiating agent). The differentiation process in CR-CSCs was monitored by assessing phosphatase alkaline activity and was more pronounced in NaB-treated CR-CSCs, as previously reported (Lucchetti et al. 2020). Differentiation was also confirmed by the reduction of the population of cells double positive for the CSC markers CD133 and CD44 by flow cytometry, as previously described (7). CR-CSCs differentiation was associated with the release of sEVs with increasing CD147 expression reaching the highest level with NaB treatment (Figure 1a; Figure S5). Thus, we referred to sEVs produced by control undifferentiated CR-CSCs (growing in suspension) as sEVs-CD147 low while we named sEVs-CD147 medium and high when the producing CR-CSCs underwent differentiation by adhesion or NaB treatment, respectively. We characterized isolated sEVs by NTA and Western blotting for the expression of CD9 and CD63 markers, as previously described (7) (Figure S1). Furthermore, we isolated CAF and NFs from colon cancer surgical samples and adjacent normal tissues (see Mate-

rials and Methods section for details). CAF displayed increased expression of the α -SMA and VIM markers compared to NFs and none of these populations expressed E-cadherin (Figure S2a,b).

First, we demonstrated that CAF can internalize sEVs labelled with CD9-PE, and that internalization occurs very rapidly and is already consistent at early time-points (10 min) (Figure 1b). Basal CD147 expression was higher in CAF than NFs and increased in proportional manner after the incubation for 48 h with sEVs with different expression of CD147 (Figure 1c; Figure S5). These data demonstrate that sEV packaged with different levels of CD147 (i.e., sEVs-CD147 low and sEVs -CD147 high) can be internalized by CAF and NFs and induce an increased expression of CD147 in recipient fibroblasts, both CAF and NCF. We showed also an increase of CD147 at the transcriptional level in recipient cells (Figure S2c). Furthermore, our findings demonstrate that CD147 expression levels could be useful in discriminating between CAF and NFs.

3.2 | CR-CSC-Released sEVs Increase the Expression of Proteins Related to Metabolism

To better understand the effect of CR-CSC-released sEV on recipient cells, we evaluated their protein content by performing a comparative proteomic analysis of sEVs-CD147 low and sEVs-CD147 high by high-resolution nano-HPLC-ESI-MS/MS. The resulting data were grouped by Venn diagram elaborations to disclose the protein elements commonly modulated in both sEV populations, considering the data obtained in triplicate LC-MS analysis of biological triplicates. The Venn diagram showed that sEVs-CD147 low were very different in protein content compared to sEVs-CD147 high: we found 324 proteins in common, while 162 proteins were exclusively expressed in sEVs-CD147 low and 252 in sEVs-CD147 high (Figure S3a).

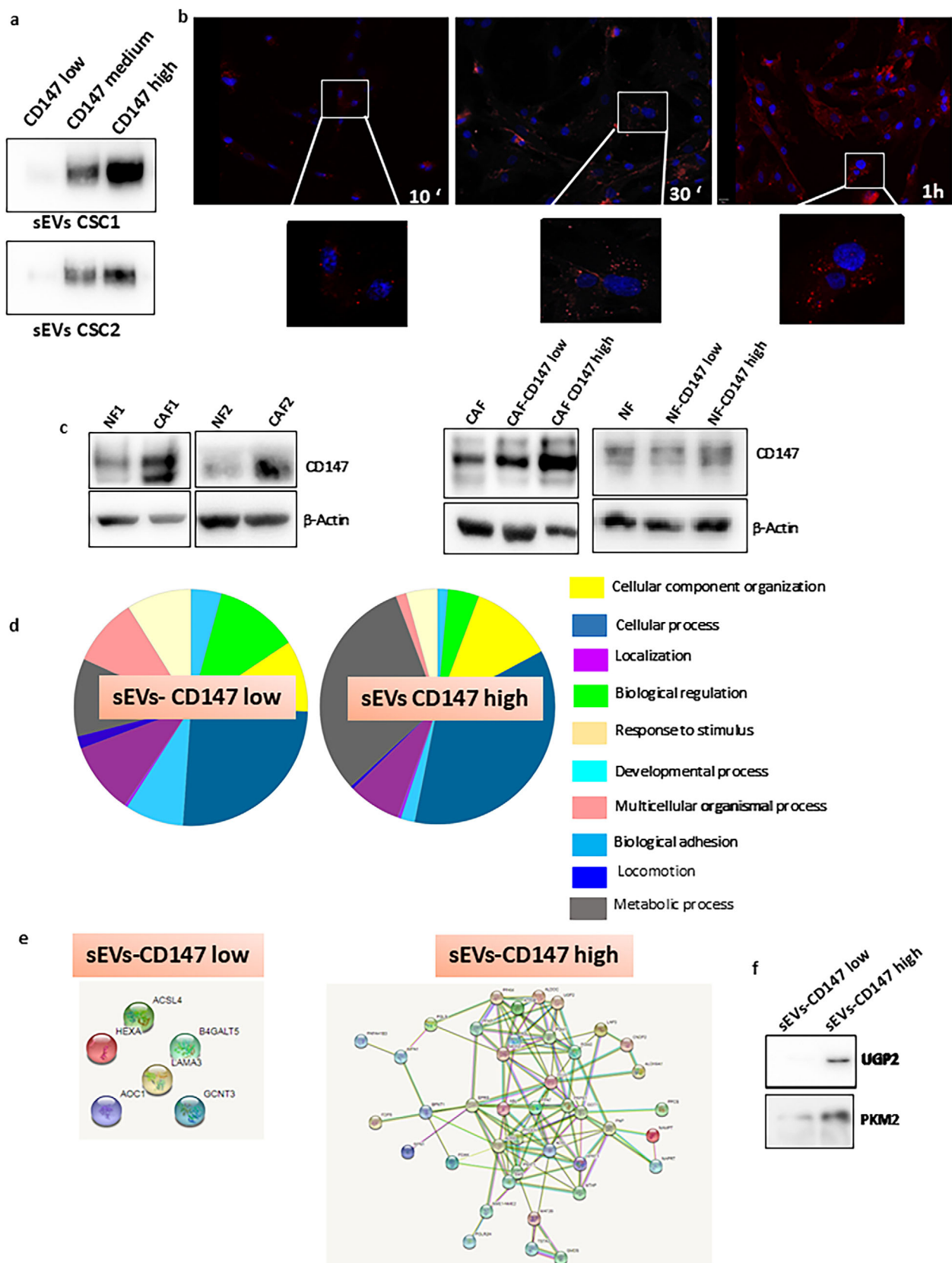


FIGURE 1 | (a) CR-CSCs produced sEVs with different CD147 expression based on the differentiation protocol used was evaluated by Western blot analysis. CD147 low = sEVs released by undifferentiated CR-CSC; CD147 medium = sEVs released by differentiated CR-CSC in adhesion condition; CD147 high = sEVs released by differentiated CR-CSC in NaB condition. (b) CAF⁺ internalization of sEVs labelled with CD9-PE at 10'–30' and 1 h. (c) Evaluation of CD147 expression is higher in CAF than NFs and its expression increases in proportional manner after the incubation for 48 h with sEVs with CD147 high. NF1 = normal fibroblast isolated from patient 1; CAF1 = cancer associated fibroblast isolated from patient 2; NF2 = normal fibroblast isolated from patient 2; CAF2 = cancer associated fibroblast isolated from patient 2; CAF = cancer associated fibroblast not conditioned with sEVs;

CAF-CD147 low = cancer associated fibroblast conditioned with sEVs at low CD147 expression; CAF-CD147 medium = cancer associated fibroblast conditioned with sEVs at medium CD147 expression; CAF-CD147 high = cancer associated fibroblast conditioned with sEVs at high CD147 expression; NF-CD147 low = normal fibroblast not conditioned with sEVs at low CD147 expression; NF-CD147 medium = normal fibroblast conditioned with sEVs at medium CD147 expression; NF-CD147 high = normal fibroblast conditioned with sEVs at high CD147 expression. (d) Mass Spectrometry of proteins in sEVs-CD147 high compared to sEVs-CD147. (e) Protein–protein interaction network analysed by STRING software. (f) Validation of enzymes related to cancer metabolism (UGP2, PKM2) to validate proteomics data.

We used the STRING and PANTHER databases to annotate the identified proteins. As expected, many of the proteins belonged to the exosomal compartment (Figure S3b). Analysis of cellular components showed that the sEVs-CD147 high were enriched in cytoplasmic and nuclear proteins compared to sEVs-CD147 low (Figure S3b). Moreover, sEVs-CD147 high appeared to be enriched in proteins involved in energy pathways, metabolism regulating pathways, transcription and translational activities (Figure 1d; Figure S3c). To validate the proteomic data, we tested by Western blot two proteins that appeared to be exclusively expressed in sEVs-CD147 low and sEVs-CD147 high, respectively: EGFR and Neu1 (Figure S4a).

Protein–protein interaction networks were also analysed using the STRING software, revealing significantly different patterns of proteins in the two sEVs populations: sEVs-CD147 high showed a cluster of highly interacting proteins related to metabolic pathways which was not evident in sEVs-CD147 low extracts (Figure 1e). In detail, the sEVs-CD147 high were enriched in enzymes related to cancer metabolism such as PFK, ALDOC, PKM2 and UGP2 (Figure 1e–f; Figure S5). Moreover, two clusters of highly interacting protein nodes detected in sEV-CD147 low were related to endocytosis and ribosome pathways (Figure S4b, left). In sEVs-CD147 high three clusters of highly interacting protein were evident and included proteins involved in the spliceosome, vesicles organization and translational pathways (Figure S4b, right).

These data suggest that vesicles released by NaB-differentiated CR-CSC, which express high levels of CD147, have a unique protein content characterized by proteins related to metabolism, spliceosome, vesicles organization and translational pathways that could affect TME (Tables 1–9).

3.3 | CR-CSC-Released sEVs Activate Fibroblasts and Modify Their Metabolomics Content

Since CAFs are crucial components of TME and undergo phenotypic changes and metabolic reprogramming ultimately impacting tumour growth, we aimed to analyse the effects of CRC-CS derived EVs on CAFs phenotype and metabolism. We observed that CR-CSC derived sEVs induced CAF activation, as confirmed by the increase of VIM, α -SMA and FAP levels. Interestingly, such effects increased with increasing differentiation of sEV-releasing cells which corresponded to increasing CD147 expression level in sEVs (Figure 2a; Figures S5 and S6). To verify whether the CD147 expressed by sEVs was involved in the observed effects on recipient fibroblasts, we pre-treated sEVs with anti-CD147 antibodies before adding them to fibroblasts cultures. We observed that this treatment almost completely abolished

the sEVs-induced effects on CAF activation markers (Figure 2b; Figures S5 and S6).

Moreover, metabolomics analyses showed that sEVs with increasing CD147 expression induced an increasing upregulation of a glycolytic phenotype in CAF, as demonstrated by the concomitant increase in lactate concentration detected in extracellular culture media and in intracellular NADH levels, the latter resulting in a consequent decrease of NAD^+/NADH ratio (Figure 2c). The metabolic switch toward the glycolytic phenotype, observed in CAF following the incubation with sEVs, was highlighted by a decrease in the intracellular ATP levels and by the concomitant increase in the intracellular ADP levels, resulting in an imbalance in the mitochondrial phosphorylating capacity, expressed as ATP/ADP ratio (Figure 2c). We observed an increase of lactate secretion in CAF exposed to sEVs with increasing CD147 expression (Figure 2c–d). These findings were associated with an increased expression of genes encoding for regulatory glycolytic enzymes, such as hexokinase (HK2), and of genes encoding for glucose and lactate transporters, such as SLC2A1 and SLC16A3, respectively (Figure 2e–g; Figure S5).

Interestingly, CAF were characterized by alterations of the reduced GSH homeostasis when exposed to CR-CSC released sEVs. In particular, CAF exhibited a parallel increase of GSH levels and decrease of the $\text{NADP}^+/\text{NADPH}$ ratio, the latter as a consequence of the increased intracellular concentration of the reduced NADPH, the cofactor necessary for the maintenance of the active reduced form of GSH (Figure 3a). Consistent with these findings, we also observed the overexpression of genes encoding for NADPH-generating enzymes, such as malic enzyme 1 (ME1) and glucose-6-phosphate dehydrogenase (encoded by G6PD), this latter suggesting a possible metabolic derangement targeting the pentose phosphate pathway (Figure 3b).

Moreover, in CAF exposed to sEVs, we detected increased levels of intracellular glycosylated UDP-derivatives, such as UDP-galactose (UDP-Gal), UDP-N-acetylglucosamine (UDP-Glc Nac) and β -pseudouridine, as indexes of increased post-translational N-linked glycosylation of proteins and of RNA turnover, respectively (Figure 3c).

3.4 | CR-CSC-Released sEVs Modify the Metabolic Status of CAF via β -Catenin and NFK β Pathways and Trigger NO-Mediated VEGF and Cytokine Secretion by Nitric Oxide Over-Production

To identify the molecular pathways involved in the modification of CAF metabolic status, we analysed those that are known to be involved in CAF activation and in the reprogramming of CAF metabolic status (3): β -catenin and NFK β pathways

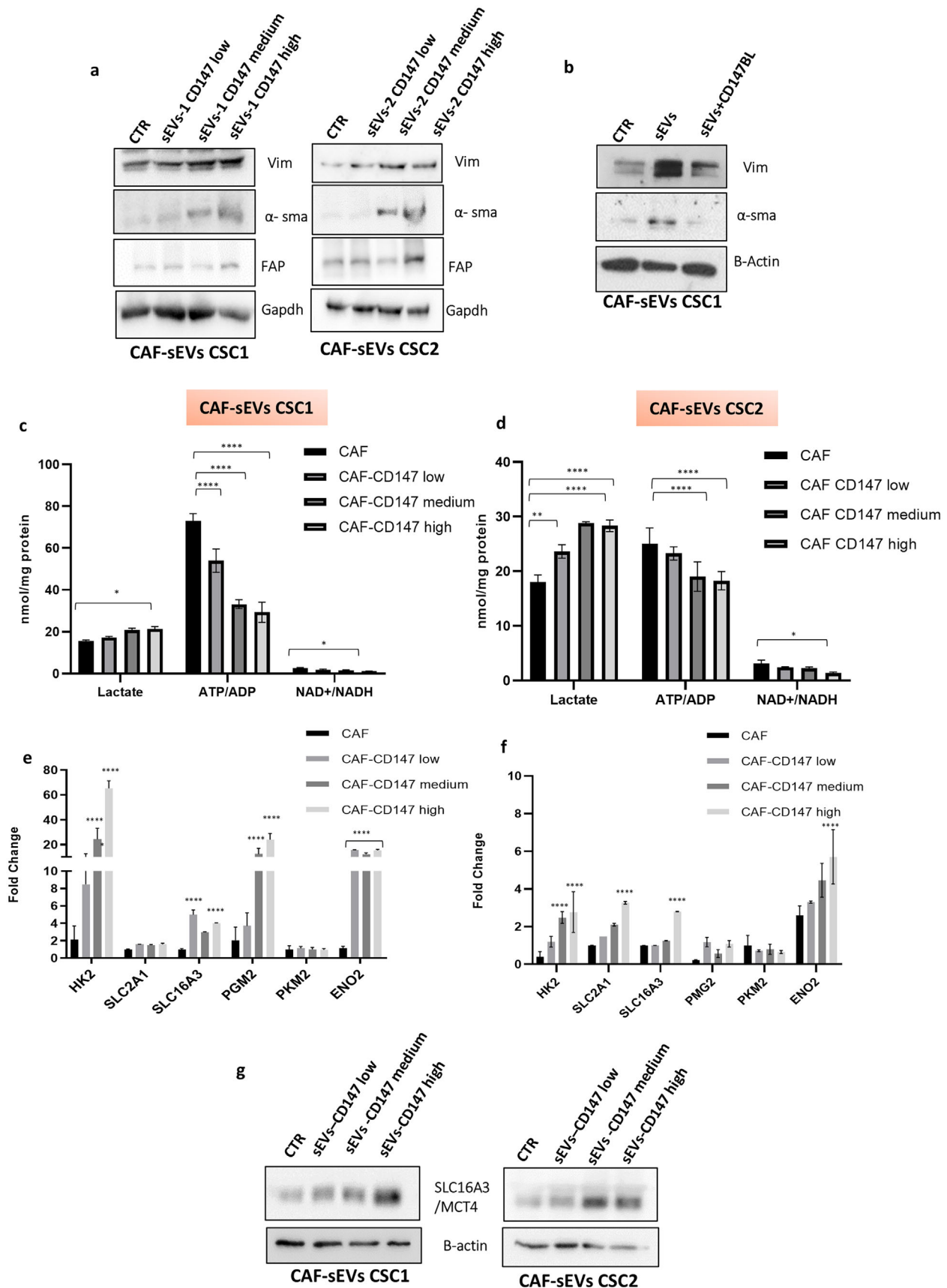


FIGURE 2 | (a) CAF activation after CR-CSC derived sEV treatment for 48 h, assessed by increase of vimentin, α -SMA and FAP levels. CTR = CAF untreated; sEVs-1 CD147 low = CAF treated with sEVs with low CD147 expression isolated from CR-CSC1; sEVs-1 CD147 medium = CAF treated with sEVs with medium CD147 expression isolated from CR-CSC1; sEVs-1 CD147 high = CAF treated with sEVs with high CD147 expression isolated from CR-CSC1; sEVs-2 CD147 low = CAF treated with sEVs with low CD147 expression isolated from CR-CSC2; sEVs-2 CD147 medium = CAF treated with

sEVs with medium CD147 expression isolated from CR-CSC2. sEVs-2 CD147 high = CAF treated with sEVs with high CD147 expression isolated from CR-CSC2. (b) Western-blot analysis of CAF activation markers after treatment with sEVs or with sEVs CD147 blocked with specific antibody. sEVs = CAF treated with sEVs-CD147 high isolated from CR-CSC1; sEVs + CD147BL = CAF treated with sEVs-CD147 high blocked by CD147 antibody isolated from CR-CSC1. (c, d) Values of extracellular lactate levels, ATP/ADP and NAD⁺/NADH intracellular ratio in CAF treated with sEVs isolated from CR-CSC1 and CR-CSC2 and expressing different CD147 levels. (e–f) Real time PCR of the gene encoding for glycolytic enzymes (HK2, PGM2, PKM2, ENO2) and genes encoding for glucose and lactate transporters (SLC2A1 and SLC16A3, respectively). (g) Western blot analysis of SLC16A3 (called also MCT4) lactate transporter in CAF conditioned with sEVs carrying different amount of CD147 release by CR-CSC1 and CR-CSC2 (sEVs–CD147 low, sEVs–CD147 medium, sEVs–CD147 high).

(Figure 4a; Figure S5). We detected an activation of β -catenin pathway that stimulated the Akt pathway and the transduction of WNT/ β -catenin target genes (such as c-Myc) to activate Hypoxia inducible factor-1 (HIF-1). Such effects increased with increasing differentiation of sEV-releasing cells which corresponded to increasing CD147 expression level present in the sEVs (Figure 4a,b). Moreover, HIF-1 α and c-Myc could be responsible for the aerobic glycolysis induction and cytosolic lactate release (Figure 2b).

To further investigate a causative link between EVs with increasing CD147 content and CAF activation we analysed the expression of NFK β , a known CAF activation factor (3). We observed an upregulation of NFK β in CAF which increased with increasing differentiation of sEV-releasing cells which corresponded to increasing sEV-CD147 expression level (Figure 4c; Figures S5–S6). To confirm the contribution of CD147 transported by sEVs in the activation of CAF and induction of the signalling pathways, we

treated sEVs with AC73, a specific inhibitor of CD147. Western blot analyses revealed that the ability of sEVs to stimulate in CAF the expression of key proteins involved in CAF activation and in metabolic modulation, such as β -catenin, NFK β , pAkt, and SLC16A3, decreased when sEVs were pre-treated with AC73 (Figure 4d; Figures S5 and S6).

It is well known that NF- κ B signalling pathway contributes to enhance the transcription of pro-inflammatory cytokines, such as IL-6 and IL-8, in cancer cells (20). We detected an increase of IL-6 and IL-8 in the supernatant of CAF conditioned for 48 h with sEVs released by NaB-differentiated CR-CSC cells expressing high levels of CD147 (Figure 4e). To confirm the specific effects of CD147 carried by sEVs, we pre-treated sEVs with an anti-CD147 antibody (1.5 μ g of antibody for 3×10^8 particles/mL) and observed that this treatment almost completely abolished the effects on the secretion of the analysed cytokines (Figure 4g). CD147 is an N-glycosylated protein so we hypothesized that this

TABLE 1 | List of cancer-related proteins identified as exclusive of sEVs-CD147 high and sEVs-CD147 low, respectively.

	UniProt accession number	Gene name	Protein description
sEVs-CD147 high	P15559	NQO1	NAD(P)H quinone dehydrogenase 1
	P62873	GNB1	G protein subunit beta 1
	Q13547	HDAC1	Histone deacetylase 1
	P01111	NRAS	NRAS proto-oncogene, GTPase
	P17612	PRKACA	Protein kinase cAMP-activated catalytic subunit alpha
	P28482	MAPK1	Mitogen-activated protein kinase 1
	Q13616	CUL1	Cullin 1
	P78417	GSTO1	Glutathione S-transferase omega 1
	O75116	ROCK2	Rho associated coiled-coil containing protein kinase 2
	P60953	CDC42	Cell division cycle 42
sEVs-CD147 low	Q14344	GNA13	G protein subunit alpha 13
	P00533	EGFR	Epidermal growth factor receptor
	P02751	FN1	Fibronectin 1
	P62993	GRB2	Growth factor receptor bound protein 2
	P61586	RHOA	Ras homologue family member A
	Q16787	LAMA3	Laminin subunit alpha 3
	P08581	MET	MET proto-oncogene, receptor tyrosine kinase
	P63208	SKP1	S-phase kinase associated protein 1
	P01137	TGFB1	Transforming growth factor beta 1

TABLE 2 | List of metabolic-related proteins identified as exclusive of sEVs-CD147 high and sEVs-CD147 low, respectively.

	UniProt accession number	Gene name	Protein description
sEVs- CD147 high	P43490	NAMPT	Nicotinamide phosphoribosyltransferase
	P14550	AKR1A1	Aldo-keto reductase family 1 member A1
	O95861	BPNT1	3'(2'), 5'-bisphosphate nucleotidase 1
	Q96DG6	CMBL	CMBL; carboxymethylenebutenolidase homologue
	P30566	ADSL	ADSL; adenylosuccinate lyase
	P30520	ADSS	ADSS; adenylosuccinate synthase
	P35573	AGL	AGL; amylo-alpha-1, 6-glucosidase, 4-alpha-glucanotransferase
	P07814	EPRS	EPRS; glutamyl-prolyl-tRNA synthetase
	P14324	FDPS	FDPS; farnesyl diphosphate synthase
	P49189	ALDH9A1	ALDH9A1; aldehyde dehydrogenase 9 family member A1
	P09972	ALDOC	ALDOC; aldolase, fructose-bisphosphate C
	O95336	PGL	PGLS; 6-phosphogluconolactonase
	O43175	PHGDH	PHGDH; phosphoglycerate dehydrogenase
	Q9NZL9	MAT2	MAT2B; methionine adenosyltransferase 2B
	P15104	GLUL	GLUL; glutamate-ammonia ligase
	O60547	GMDS	GMDS; GDP-mannose 4,6-dehydratase
	P17174	GOT1	GOT1; glutamic-oxaloacetic transaminase 1
	Q9Y617	PSAT1	PSAT1; phosphoserine aminotransferase 1
	P00492	HPRT1	HPRT1; hypoxanthine phosphoribosyltransferase 1
	P51659	HSD17B4	HSD17B4; hydroxysteroid 17-beta dehydrogenase 4
	P29218	IMPA1	IMPA1; inositol monophosphatase 1
	P40926	MDH2	MDH2; malate dehydrogenase 2
	P04424	ASL	ASL; argininosuccinate lyase
	Q13126	MTAP	MTAP; methylthioadenosine phosphorylase
	P00491	PNP	PNP; purine nucleoside phosphorylase
	Q15102	PAFAH1B3	PAFAH1B3; platelet activating factor acetylhydrolase 1b catalytic subunit 3
	P06576	ATP5F1B	ATP5F1B; ATP synthase F1 subunit beta
	P28838	LAP3	LAP3; leucine aminopeptidase 3
	P08237	PFKM	PFKM; phosphofructokinase, muscle
	Q01813	PFKP	PFKP; phosphofructokinase, platelet
	P36871	PGM1	PGM1; phosphoglucomutase 1

(Continues)

TABLE 2 | (Continued)

UniProt accession number	Gene name	Protein description
P52434	POLR2H	POLR2H; RNA polymerase II subunit H
Q06203	PPAT	phosphoribosyl pyrophosphate amidotransferase
Q96G03	PGM2	PGM2; phosphoglucomutase 2
Q96KP4	CNDP2	CNDP2; carnosine dipeptidase 2
P60891	PRPS1	PRPS1; phosphoribosyl pyrophosphate synthetase 1
P04843	RPN1	RPN1; ribophorin I
P22392	NME1-NME2	NME1-NME2 readthrough
P52788	SMS	Spermine synthase
Q13630	TSTA3	Tissue specific transplantation antigen P35B
Q16851	UGP2	UDP-glucose pyrophosphorylase 2
Q9HAB8	PPCS	Phosphopantothenoylcysteine synthetase
O00764	PDXK	Pyridoxal kinase
P42330	AKRIC3	Aldo-keto reductase family 1 member C3
Q6XQN6	NAPRT	Nicotinate phosphoribosyltransferase
P43490	ACSL4	Acyl-CoA synthetase long chain family member 4
P14550	AOC	Amine oxidase, copper containing 1
O95861	HEXA	Hexosaminidase subunit alpha
Q96DG6	LAMA3	Laminin subunit alpha 3
P30566	GCNT	Glucosaminyl (N-acetyl) transferase 3, mucin type
P30520	B4GALT5	Beta-1,4-galactosyltransferase 5

post-translational modification may be involved in sEVs-induced effects on recipient cells. In support of this hypothesis, we observed that reducing sEVs N-glycosylation by N-glycosidase pre-treatment (as described in Material and Methods) of sEVs prevented the increase of IL-6 and IL-8 release in conditioned medium of sEV-treated CAF (Figure 4f).

Given that lactate has been reported to induce VEGF secretion, we analysed its expression in CAF conditioned with sEVs, and, again, we observed a progressive increase with differentiation of sEV-releasing cells which corresponded to higher CD147 expression level on sEVs (Figure 5a; Figures S5 and S6). Several pieces of evidence suggest that nitrogen oxide (NO) promotes HIF-1 α stabilization enhancing the effects of hypoxia in promoting tumour neoangiogenesis (21). Thus, we analysed NO cargo in sEVs, showing an increase in the concentration of the end products of its metabolism (NO₂ and NO₃) with a concomitant increase of NO secretion in CAF conditioned by EVs that increased with increasing sEV-CD147 expression level (Figure 5b). VEGF and NO are two important modulators of angiogenesis (Taniguchi and Karin 2018). For this reason, we used HUVEC to assess

the ability of CR-CSC-released sEVs to induce angiogenesis, as assessed using the endothelial tube formation assay. We observed that CR-CSC-released sEVs were able to induce tube formation and that the ability of HUVEC cells to establish a dense network of nodes and junctions reached the highest levels when cells were incubated with sEVs-CD147 high, released by NaB-differentiated CR-CSC cells, compared to untreated cultures or treated with EVs expressing lower levels of CD147 (Figure 5c).

3.5 | CR-CSC-Released sEVs Promote the Invasion of CSC In Vitro and Tumour Growth In Vivo

Having shown that sEVs protein content is different based on the degree of differentiation of the releasing CR-CSCs, which correlated with sEVs-CD147 expression level, we next sought to determine whether CD147 carried by sEVs might affect CRC cells migration and invasion. To this aim, we first used HCT116 CRC cells to set up a Boyden chamber-based transwell invasion assay using CR-CSC-released sEV as a chemoattractant. We observed a striking increase of invading cells induced by sEVs

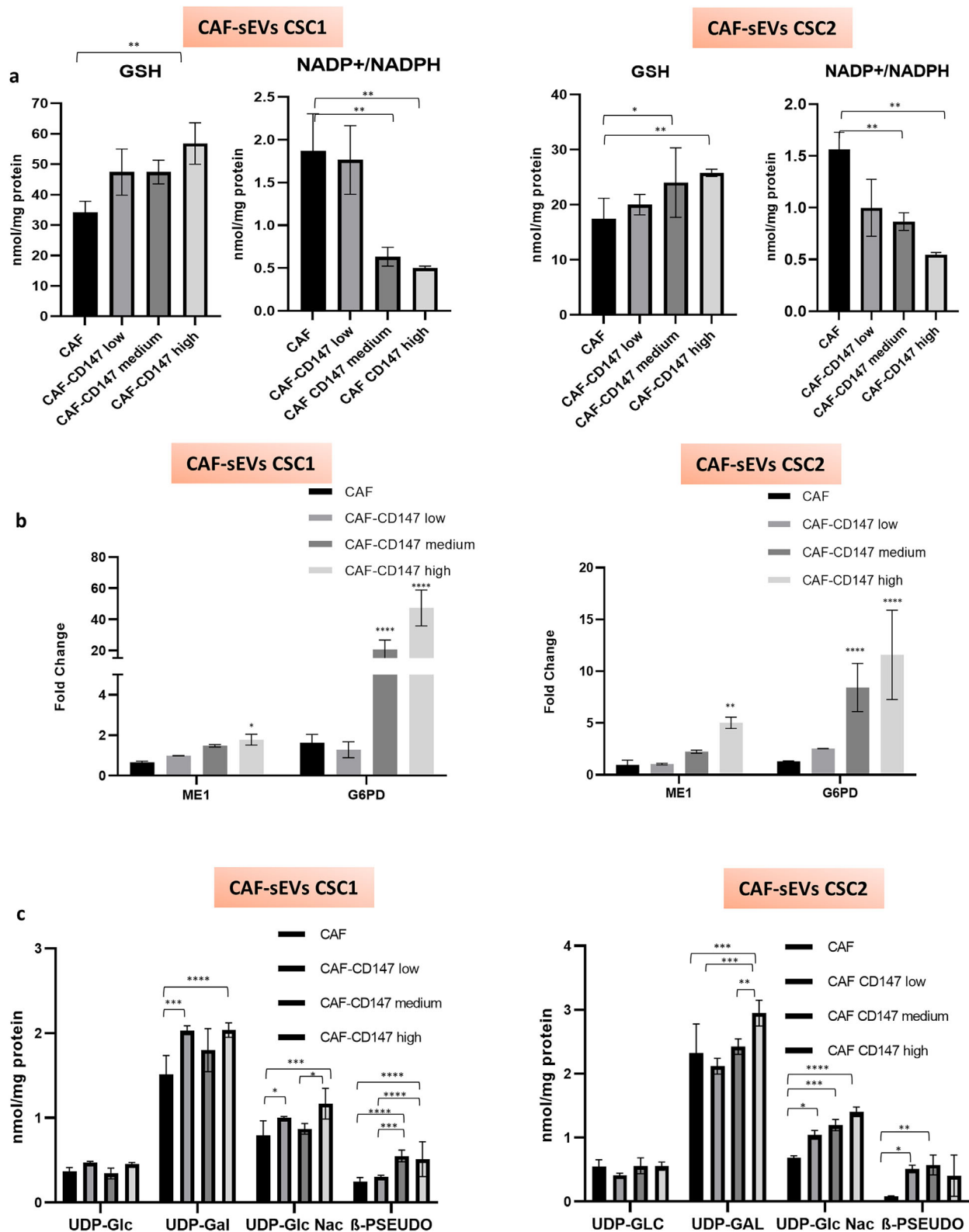


FIGURE 3 | (a) Intracellular levels of GSH and NADP⁺/NADPH in CAF treated by sEVs with different levels of CD147 isolated from CR-CSC1 and CR-CSC2. (b) Evaluation of gene expression encoding the for NADPH-generating enzymes, as ME1 and G6PD. (c) Evaluation of intracellular glycosylated UDP-derivatives, as UDP-Gal, UDP-Glc Nac and of β-pseudouridine, as indexes of increased post-translational N-linked glycosylation of proteins and of RNA turnover, respectively.

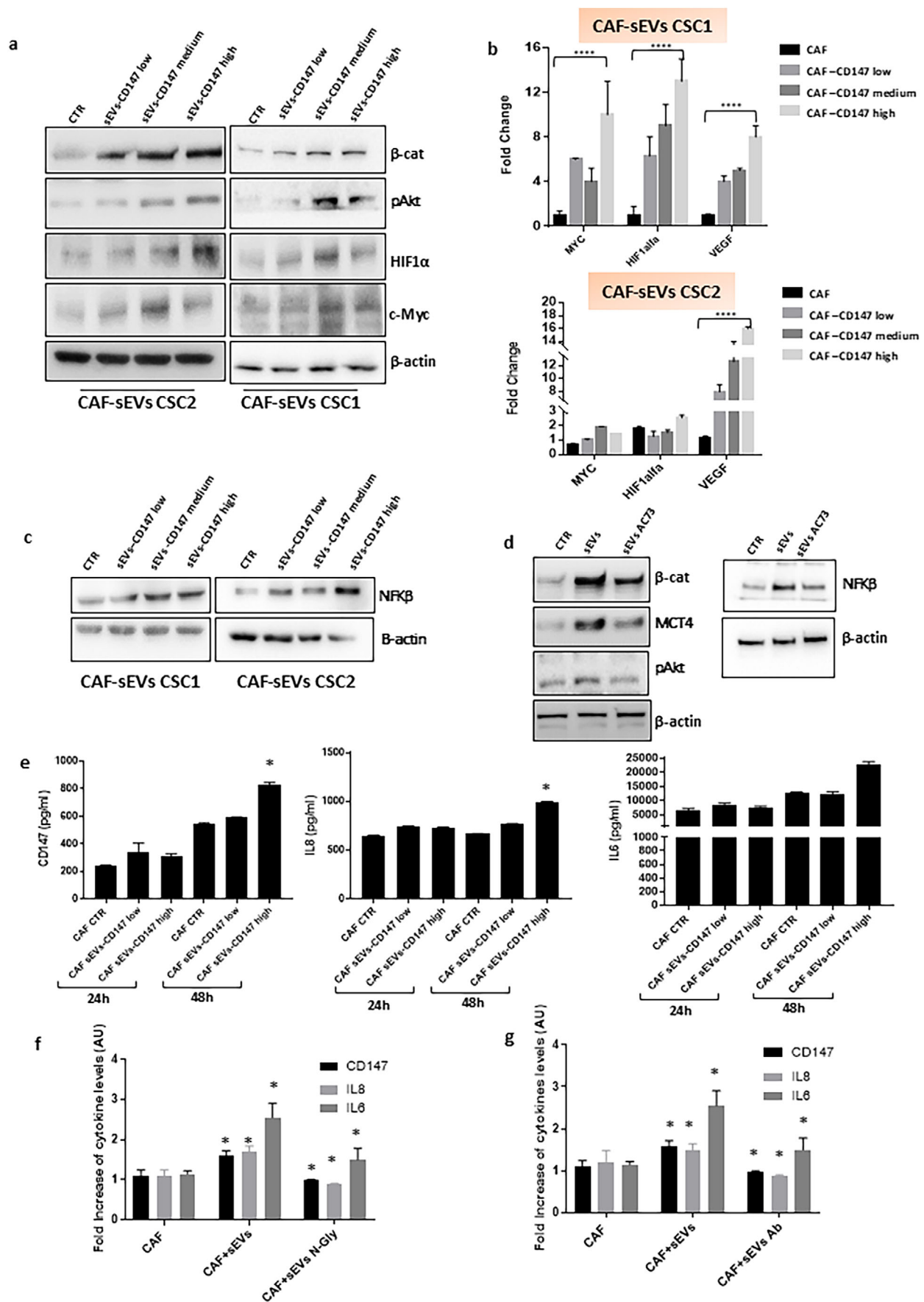


FIGURE 4 | (a–c) Western blot analysis of β -catenin, pAkt, HIF1 α , c-Myc and NFK β and gene expression of Myc, HIF1 α and VEGF in CAF conditioned by sEVs with growing CD147 content. (d) Western blot analyses revealed that CAF treated with CD147 sEVs pre-treated with AC73 underwent

a reduction of some key proteins involved in CAF activation and in metabolism modulation (β -catenin, NFK β , pAkt, SLC16A3). (e) Analysis of pro-inflammatory cytokines such as IL-6 and IL-8 and CD147 soluble form by Luminex assay in supernatant of CAF conditioned by sEVs with growing CD147 content at 24 and 48 h. (f) sEVs pre-treated with anti-CD147 antibodies or deleting its N-glycosylation to analyse the CAF treatments to evaluate the secretion of analysed cytokines.

compared to control cells (in the absence of sEVs), and this effect increased with increasing differentiation of sEV-releasing cells, which corresponded to increasing sEVs-CD147 expression level (Figure 6a). Based on the above findings, we set out to explore whether sEVs induced changes in the phosphorylation status of intracellular proteins. We performed an immunoblot analysis of phosphorylated tyrosine (p-Tyr), and we observed an increase in the level of tyrosine phosphorylation in CSC cells treated with CR-CSC-derived sEVs correlating with the degree of differentiation of sEV-releasing cells and sEVs-CD147 expression level, suggesting that CD147 might be involved in the activation of intracellular signalling pathways in recipient cells (Figure 6b). In addition, sEVs-CD147 high were able to induce the phosphorylation of tyrosine residues at earlier time points (5 min) compared to sEVs-CD147 low, and the effect did not augment by increasing the amount of EVs administered (Figure 6b).

In order to investigate whether and how CR-CSC-released sEV could affect CSC growth in vivo, we used an in vivo tumorigenesis model in the flank of NOD/SCID/IL2R γ -null (NSG) mice by injecting CR-CSCs suspensions untreated or pretreated with sEVs. First, using the Boyden chamber-based transwell invasion assay, we confirmed that CR-CSC invasion ability increased using CR-CSC-released sEVs and that, as demonstrated for HCT116 cells, this effect increased with increasing sEVs-CD147 expression level (Figure 6d). To determine the timing of CR-CSCs pre-treatment with sEVs before the inoculation in vivo, we specifically analysed the expression of pERK, a well-known modulator of cell proliferation, migration and invasion, in sEVs-treated cells (Figure 6c) following the administration schedule depicted in Figure 6c (Day 1, sEVs treatment; Day 4, sEVs treatment; Day 7, proteins collection or cell invasion assay). Once the treatment scheme to be used in vivo was determined, we implanted the CRC-CSC in the flank of NSG mice and observed that subcu-

TABLE 3 | List of proteins processing in endoplasmic reticulum identified as exclusive of sEVs-CD147 high and sEVs-CD147 low, respectively.

	UniProt accession number	Gene name	Protein description
sEVs-CD147 high	Q15084	PDIA6	Protein disulfide isomerase family A member 6
	Q15436	SEC23A	Sec23 homologue A, coat complex II component
	P05198	EIF2S1	Eukaryotic translation initiation factor 2 subunit alpha
	P07237	P4HB	Prolyl 4-hydroxylase subunit beta
	P04843	RPN1	Ribophorin I
	Q8NBS9	TXNDC5	Thioredoxin domain containing 5
	P07384	CAPN1	Calpain 1
	Q13616	CUL1	Cullin 1
	O95816	BCL2	BCL2 associated athanogene 2
	P53992	SEC24C	SEC24 homologue C, COPII coat complex component
sEVs-CD147 low	Q15084	PDIA6	Protein disulfide isomerase family A member 6
	Q15436	SEC23A	Sec23 homologue A, coat complex II component
	P05198	EIF2S1	Eukaryotic translation initiation factor 2 subunit alpha
	P07237	P4HB	Prolyl 4-hydroxylase subunit beta
	P04843	RPN1	Ribophorin I
	Q8NBS9	TXNDC5	Thioredoxin domain containing 5
	P07384	CAPN1	Calpain 1
	Q13616	CUL1	Cullin 1
	O95816	BCL2	BCL2 associated athanogene 2
	P53992	SEC24C	SEC24 homologue C, COPII coat complex component

TABLE 4 | List of protein processing in endoplasmic reticulum identified as exclusive of sEVs-CD147 high and sEVs-CD147 low, respectively.

	UniProt accession number	Gene name	Protein description
sEVs- CD147 high	Q15084	PDIA6	Protein disulfide isomerase family A member 6
	Q15436	SEC23A	Sec23 homologue A, coat complex II component
	P05198	EIF2S1	Eukaryotic translation initiation factor 2 subunit alpha
	P07237	P4HB	Prolyl 4-hydroxylase subunit beta
	P04843	RPN1	Ribophorin I
	Q8NBS9	TXNDC5	Thioredoxin domain containing 5
	P07384	CAPN1	Calpain 1
	Q13616	CUL1	Cullin 1
	O95816	BAG2	BAG family molecular chaperone regulator 2
	P53992	SEC24C	SEC24 homologue C
sEVs- CD147 low	O60884	DNAJA2	DnaJ homologue subfamily A member 2
	Q9Y4L1	HYOU1	Hypoxia up-regulated 1
	P31689	DNAJA1	DnaJ homologue subfamily A member 1
	P63208	SKP1	S-phase kinase-associated protein 1

TABLE 5 | List of spliceosome-related proteins identified as exclusive of sEVs-CD147 high.

	UniProt accession number	Gene name	Protein description
sEVs- CD147 high	Q6P2Q9	PRPF8	Pre-mRNA processing factor 8
	Q86XP3	DDX42	DEAD-box helicase 42
	P17844	DDX5	DEAD-box helicase 5
	O43143	DHX15	DEAH-box helicase 15
	O75533	SF3B1	Splicing factor 3b subunit 1
	Q9UMS4	PRPF19	Pre-mRNA processing factor 19
	Q09161	NCBP1	Nuclear cap binding protein subunit 1
	Q96E39	RBMXL1	RBMX like 1
	Q07955	SRSF1	Serine and arginine rich splicing factor 1

taneous (sc) xenografts grew more rapidly when CR-CSC were pretreated with CR-CSC-released sEVs and that tumour growth enhancement was stronger with sEVs-CD147 high compared to sEVs-CD147 low (Figure 6e,f).

3.6 | Activation of Fibroblasts by CR-CSC-Released sEV Promote Cancer Growth In Vivo

To determine whether CR-CSC-released sEV-mediated CAF reprogramming could also contribute to tumour growth in vivo, we preliminarily assessed the effect of conditioned medium (CM)

of CAF pre-treated with sEVs carrying different amounts of CD147 on HCT116 and CR-CSC1 invasion using the previously described Boyden chamber-based transwell invasion assay. As expected, CM from CAF resulted in a robust increase of invasion ability in both HCT116 and CR-CSC1 cells, and this effect increased with increasing differentiation of sEV-releasing cells, which corresponded to increasing sEV-CD147 expression level (Figure 7a,b). Moreover, to test the cellular behaviour and natural interactions between CAF and cancer cells, we performed a co-culture of CR-CSC cells and CAF using control, untreated CAF or CAF pretreated with sEVs. We observed, by quantifying the number of CAF at the interface with HT29 cells, that cell interaction between CAF and HT29

TABLE 6 | List of vesicles organization-related proteins identified as exclusive of sEVs-CD147 high.

	UniProt accession number	Gene name	Protein description
sEVs- CD147 high	P61923	COPZ1	Coatomer subunit zeta-1
	O60763	USO1	General vesicular transport factor
	O14579	COPE	Coatomer subunit epsilon
	P53621	COPA	Coatomer subunit alpha
	O15498	YKT6	Synaptobrevin homologue
	Q15436	SEC23A	Protein transport protein
	P62820	HRAB1A	Ras-related protein
	P48444	ARCN1	Coatomer subunit delta

TABLE 7 | List of translational pathway-related proteins identified as exclusive of sEVs-CD147 high.

	UniProt accession number	Gene name	Protein description
sEVs- CD147 high	P62701	RPS4X	40S ribosomal protein S4, X isoform
	O15372	EIF3H	Eukaryotic translation initiation factor 3 subunit H
	P62753	RPS6	40S ribosomal protein S6
	P30050	RPL12	60S ribosomal protein L12
	P62277	RPS13	40S ribosomal protein S13
	Q9BY44	EIF2A	Eukaryotic translation initiation factor 2A
	P20042	EIF2S2	Eukaryotic translation initiation factor 2 subunit 2
	P15880	RPS2	40S ribosomal protein S2
	P62888	RPL30	60S ribosomal protein L30
	Q99613	EIF3C	Eukaryotic translation initiation factor 3 subunit C
	P41091	EIF2S3	Eukaryotic translation initiation factor 2 subunit 3
	P25398	RPS12	40S ribosomal protein S12
	P04843	RPN1	Dolichyl-diphosphooligosaccharide-protein glycosyltransferase subunit 1
	P05198	EIF2S1	Eukaryotic translation initiation factor 2 subunit 1
	P46782	RPS5	40S ribosomal protein S5

cells increased when CAF had been pretreated with sEVs and that this effect increased with increasing sEV-CD147 expression level. Moreover, when CAF had been pretreated with sEVs, the morphology of both cell lines changed, compared to co-culture with control CAF, appearing more elongated (Figure 7c). Based on these interesting pieces of evidence, we aimed to investigate the effects of CAF pretreatment with sEVs on the in vivo tumour growth of CR-CSC1 cells. We used the previously described in vivo tumorigenesis model in the flank of NSG mice by co-injecting CAF with CR-CSCs. CAF were used untreated (only with vehicle) or pre-treated for 72 h with sEVs and were injected with CR-CSC1 in mice at Day 0, followed at Days 7, 14, and

21 by the peritumoral injection of sEVs-CD147 low, and high. Mice were sacrificed at 27 days after cells inoculation, and we observed that tumour volume was not significantly affected by CAFs as well as by CAF conditioned with sEVs-CD147 low but it strikingly increased in mice inoculated with cells suspensions containing CAF conditioned with sEVs-CD147 high (Figure 7d,e; Figure S7). In order to evaluate fibroblasts activation and their metabolic status in vivo and the degree of fibroblasts-cancer cells interactions in vivo, we analysed the tumours by Opal multiplex immunofluorescence based on TSA amplification to reveal the spatial context of cell-cell interactions in the tissue (Figure 8a). First, we accounted the number of PANCK+ CD147+

TABLE 8 | List of endocytosis-related proteins identified as exclusive of sEVs-CD147 low.

	UniProt accession number	Gene name	Protein description
sEVs- CD147 low	O43633	CHMP2A	Charged multivesicular body protein 2a
	Q9NZZ3	CHMP5	Charged multivesicular body protein 5
	Q9UK41	VPS28	Vacuolar protein sorting-associated protein 28
	Q86VN1	VPS36	Vacuolar protein-sorting-associated protein 36
	Q96H20	SNF8	Vacuolar-sorting protein SNF8
	Q9UQN3	CHMP2B	Charged multivesicular body protein 2b
	Q9H9H4	VPS37B	Vacuolar protein sorting-associated protein 37B
	Q9BRG1	VPS25	Vacuolar protein-sorting-associated protein 25

TABLE 9 | List of ribosomes-related proteins identified as exclusive of sEVs-CD147 low.

	UniProt accession number	Gene name	Protein description
sEVs- CD147 low	P62424	RPL7A	Ribosomal protein L7a
	P30050	RPL12	Ribosomal protein L12
	P62888	RPL30	Ribosomal protein L30
	P15880	RPS2	Ribosomal protein S2
	P62701	RPS4X	Ribosomal protein S4 X-linked
	P46782	RPS5	Ribosomal protein S5
	P62753	RPS6	Ribosomal protein S6
	P25398	RPS12	Ribosomal protein S12
	P62277	RPS13	Ribosomal protein S13
	P62424	RPL7A	Ribosomal protein L7a

cancer cells and observed their increase in sEVs treated tumours proportionally to their CD147 expression level. It is already known that lactate, produced by CAF expressing monocarboxylate transporter 4 (MCT-4), is released in the extracellular milieu and subsequently internalized and utilized by tumour cells through the increased expression of monocarboxylate transporter 1 (MCT-1) (López-Sánchez et al. 2020). Based on these published pieces of evidence, we analysed the expression of MCT1 in tumour cells (PANCK+CD147+MCT1+) and confirmed its increase in tumour obtained with sEVs treated CR-CSC cells, compared to control untreated CR-CSCs, and this effect increased with increasing sEVs-CD147 expression level. Moreover, we found an increase of CAF positive for MCT4, further supporting the molecular mechanism of lactate export (Figure 8b). To confirm

the CAF activation, we used the FAP marker in addition to α -SMA and we observed a drastic increase of activated FAP+CD147+ cells in tumours injected with CAF conditioned by sEVs-CD147-high (Figure 8b). Definitely, we confirmed the higher cell-cell interactions between CAF CD147+MCT4+ and PANCK+MCT1+ cancer cells in tumour obtained by injection with sEV-treated CR-CSC cells and this effect increased with increasing sEVs-CD147 expression level as well as the nearest cell populations of activated CAF and CD147-PANCK1 tumour cells (Figure 8c). Moreover, we determined the *h*-score of membrane CD147 that resulted in an increase in both stroma and tumour compartment (Table 2). These data confirmed that fibroblast activation and their metabolic status in vivo and the degree of fibroblast-cancer cells interactions in vivo are affected by sEVs released

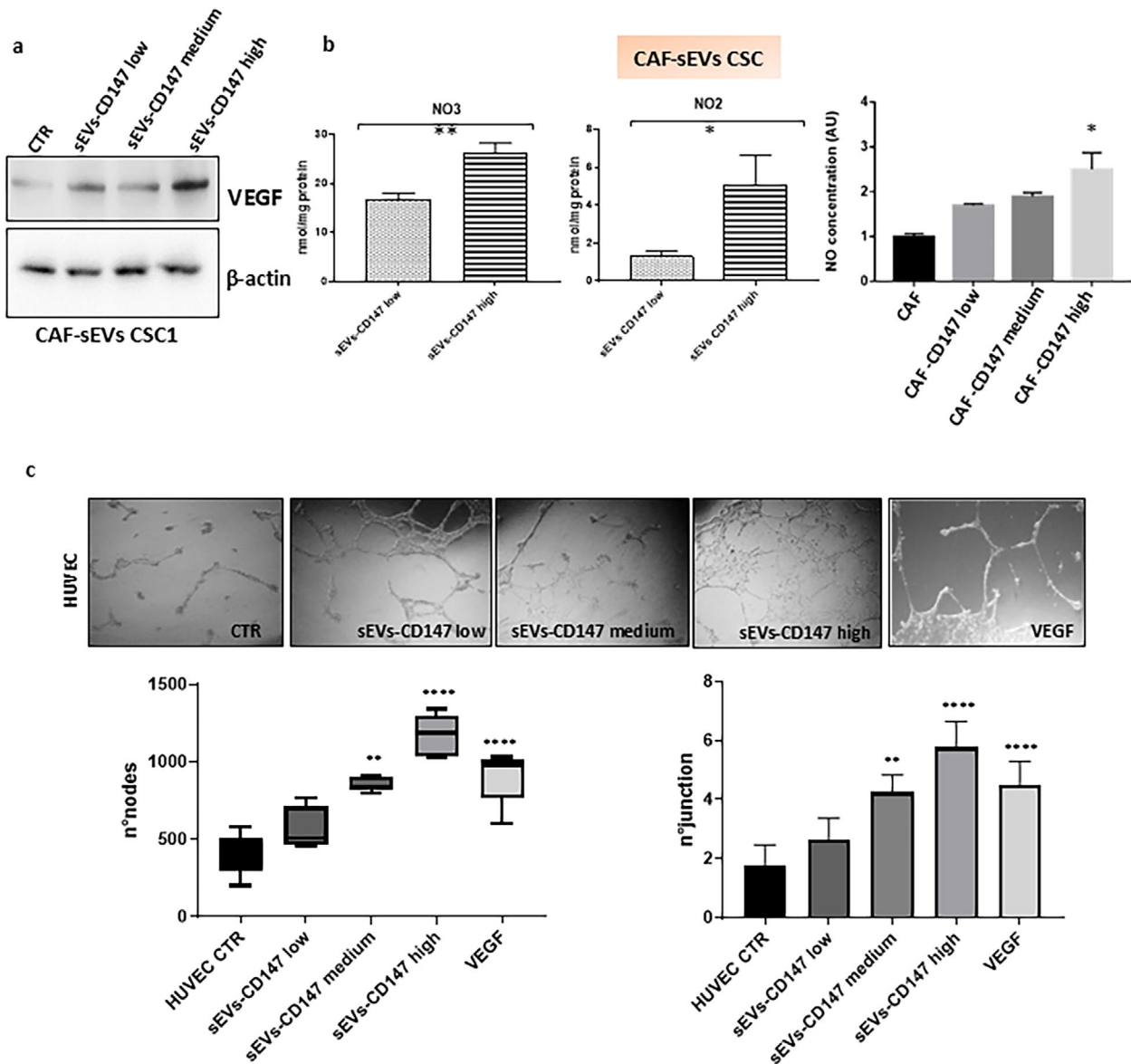


FIGURE 5 (| a) Analysis of VEGFA expression in CAF conditioned with sEVs with differential expression of CD147. (b) Evaluation of nitrogen oxides cargo in sEVs-CD147 low and sEVs-CD147 high (left) and NO levels in CAF conditioned by EVs with increasing amount of CD147. (c) HUVEC tube formation assay. The sEVs-CD147 high induce the HUVEC to establish a dense network of nodes and junctions compared to untreated or treated with EVs-CD147 low.

by CR-CSC cells undergoing differentiation and increase with their increasing differentiation and the corresponding increasing expression of CD147 on EVs.

4 | Discussion

CSCs constitute a small fraction within the overall tumour mass, playing a crucial role in sustaining tumour growth and evading anticancer treatments (Greaves and Maley 2012; Lucchetti et al. 2020). Their involvement in tumour recurrence and metastasis significantly impacts prognosis and clinical outcome of cancer patients. Although the mechanisms through which CSCs exert these effects are still debated, numerous studies suggest that they develop reciprocal interactions with cells within TME, with TME normal cells providing a supportive niche for CSC survival and

self-renewal, while CSCs, in turn, can influence the polarization and metabolism of cells in TME. It is not clear how CSCs exert these effects, but several pieces of evidence suggest that they could produce factors, including EVs, able to modulate the behaviour of TME, inducing it to become supportive for cancer cells to develop, escape from host immune surveillance and resist anticancer therapies.

Previously, we showed that sEV secretion during CR-CSC differentiation is partially controlled by CD147 and that CD147-sEVs activate a signalling cascade in recipient tumour cells, inducing molecular invasive features of CSCs (Lucchetti et al. 2017; Lucchetti et al. 2020). In the present study, we analysed the effects of CR-CSC-released EVs on TME and demonstrate that they are able to increase the expression of myofibroblast and activation markers in CAF. It is noteworthy that we observed similar effects

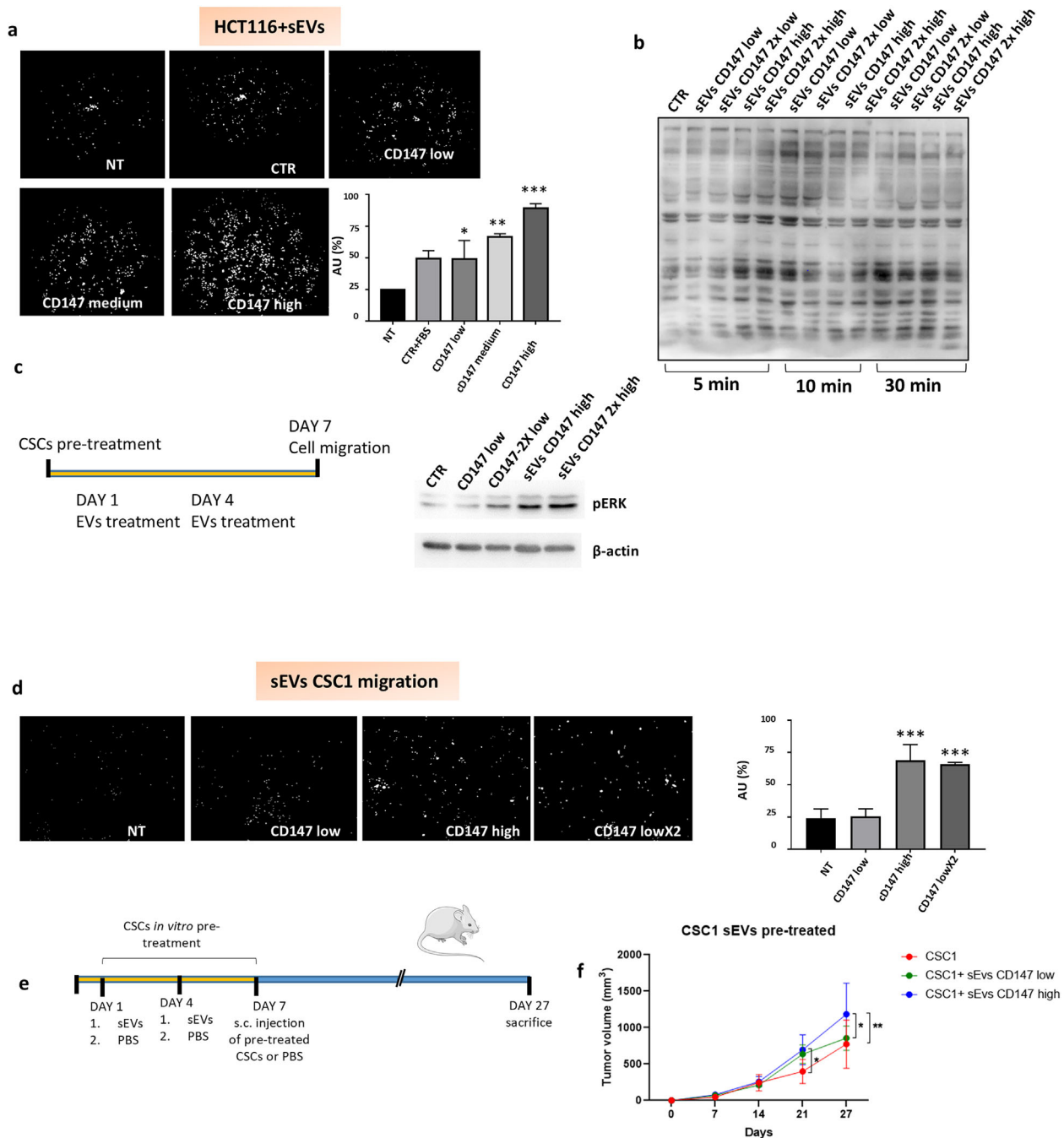


FIGURE 6 | (a) HCT116 cells were seeded onto the upper chamber of each Transwell insert of 96 well plate Corning FluoroBlok. The lower chamber was filled with different medium conditions to serve as chemoattractants for cell invasion: (1) only medium (NT); (2) medium + FBS (CTR); (3) medium + sEVs CD147 low released by CR-CSC1 (CD147 low); (4) medium + sEVs CD147 medium released by CR-CSC1 (CD147 medium); (5) medium + sEVs CD147 high (CD147 high) released by CR-CSC1. Calcein fluorescence was evaluated by fluorescent plate reader. Representative images and relative quantification were shown. (b) Immunoblot analysis of phosphorylated tyrosine (p-Tyr) in CSC1 cells treated with CR-CSC-derived sEVs with differential expression of CD147 at 5', 10', and 30'. Phosphorylated tyrosine was evaluated also after administration of double concentration of sEVs in HCT116 (sEVs 2x). (c) Expression of pERK in sEV-treated CR-CSC1 cells and following the administration schedule (Day 1, sEVs treatment; Day 4 sEVs treatment; Day 7 proteins collection or cell migration assay); sEVs used for the treatment were isolated from CR-CSC1 with specific protocols to obtain different expression of CD147 (see Material and Methods section). (d) Migration assay of CR-CSC1 performed by 96 well plate Corning FluoroBlok. CR-CSC1 cells were treated at Days 1, 4, and 7 with sEVs expressing different amount of CD147. Conditioned CR-CSC1 cells were dissociated, counted and plated in 96 well to perform migration at 24 h. (e-f) CR-CSC1 pretreated with EVs derived from CR-CSC1 on Days 1 and 4. After 7 of culture CRC-SCs were dissociated, resuspended in 50% PBS/50% Matrigel and injected subcutaneously (5×10^5 cells/mouse) in the flank of NSG mice ($n = 6$). Xenografts were measured once a week by digital calliper, and volumes were calculated using the following formula: $\pi/6 \times d^2 \times D$ (left).

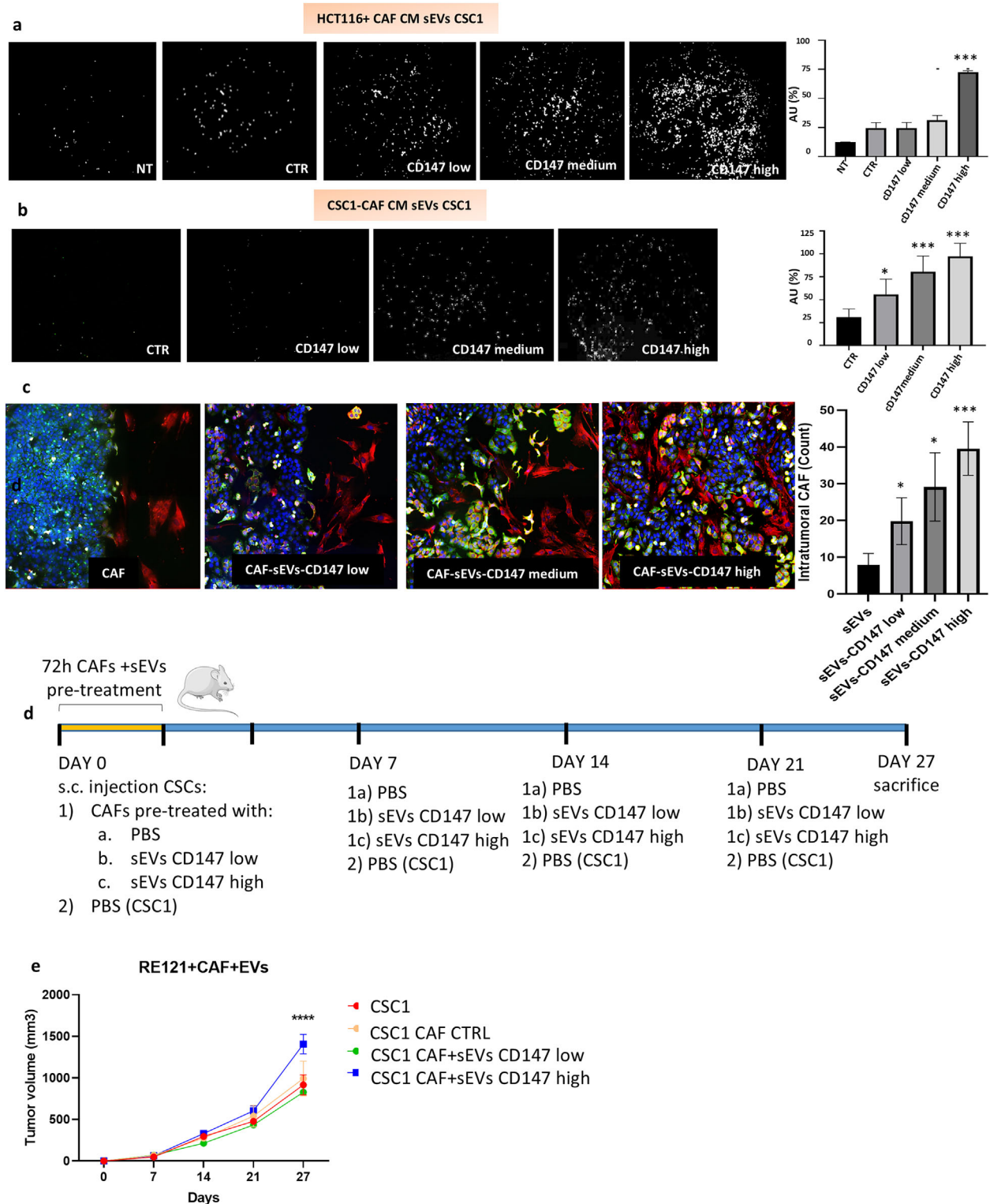


FIGURE 7 | (a–b) HCT116 and CR-CSC1 cells were seeded onto the upper chamber of each Transwell insert of 96 well plate Corning FluoroBlok. For HCT116, the lower chamber was filled with different medium conditions to serve as chemoattractants for cell invasion: (1) NT: fresh medium without FBS; (2) CTR: fresh medium + FBS; (3) CD147 low: medium of CAF conditioned for 48 h with sEVs CD147 low; (4) CD147 medium: medium of CAF conditioned for 48 h with sEVs CD147 medium; (5) CD147 high: medium of CAF conditioned for 48 h with sEVs CD147 high. For CR-CSC1: CTR: fresh medium+ FBS; (2) CD147 low: medium of CAF conditioned for 48 h with sEVs CD147 low; (3) CD147 medium: medium of CAF conditioned for 48 h with sEVs CD147 medium; (4) CD147 high: medium of CAF conditioned for 48 h with sEVs CD147 high. (c) Immunofluorescence images of HT29 and CAF coculture. Blue = DAPI; red: α -SMA; green: phalloidin; magnification: 20 \times . (d–f) CAF pre-treated for 72 h with sEVs were injected with CR-CSC1 in six mice (Day 0) and at 7–14 and 21 days after cell injection we inoculated peritumorally sEVs CD147 low or high. Xenografts were measured once a week by digital calliper, and volumes were calculated using the following formula: $\pi/6 \times d^2 \times D$ (left). Tumour volume at Day 27 (right).

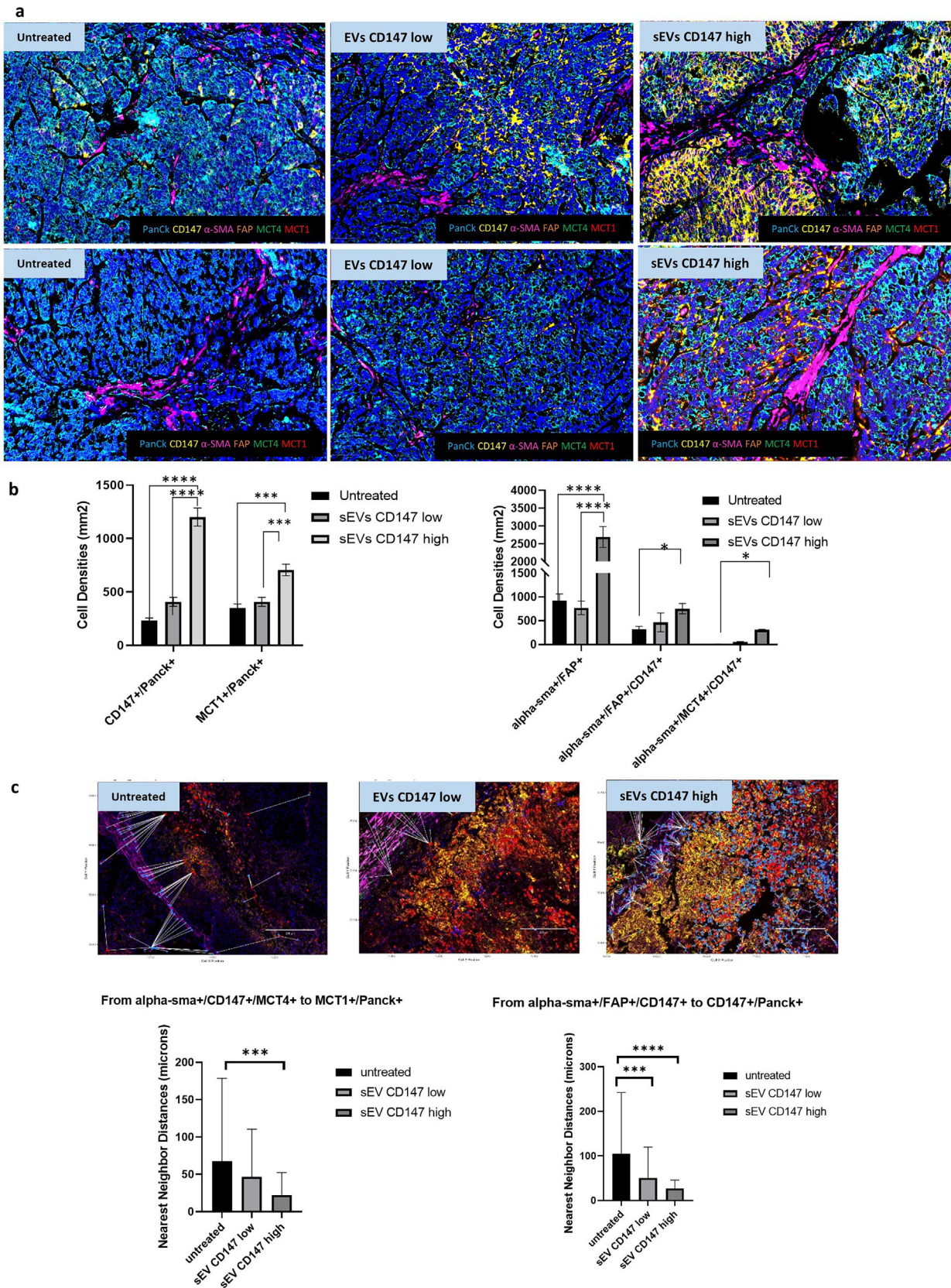


FIGURE 8 | Multiplex spatial imaging in the mouse model transplanted with CAF conditioned with sEVs carrying different amount of CD147 and CR-CSC1. (a) Representative seven-colour multispectral images of mouse sample stained with the mIF panel. Original magnification 20×. Immune markers and colour codes are indicated in the legend. (b) Significant differences in cell population (CD147+/Panck+; MCT1+/Panck+; α-SMA/FAP+; α-SMA/FAP+/CD147+; α-SMA/MCT4+/CD147+) analysed according to mice groups described above. Data are presented as cell density (number of cells/mm²). (c) Mean distance (μm) between: (1) Each PANCK-MCT1 tumour cell and the nearest MCT4 CAF cells. (2) Each PANCK-MCT1 tumour cell

on CAF by exposing them to sEVs isolated from other CSC with different genetic backgrounds (Lucchetti et al. 2020) (data not shown).

Moreover, we demonstrated that CR-CSCs induced to differentiate produced sEVs with increasing CD147 expression that reached the highest when cells were induced to differentiate by growing them to confluence and exposing them to NaB (7, Figure 1a). We showed that CR-CSC-released EVs induced an increase of the α -SMA and FAP expression in CAF and that this effect increased with increasing differentiation of sEV-releasing cells, which corresponded to increasing sEV-CD147 expression level. These findings suggested that CD147 might play an important role in EVs-induced effects on recipient CAF, as demonstrated by the observation that blocking CD147 on the surface of sEVs largely abolished their effects on recipient cells.

It is well described that the Wnt/ β -catenin pathway can induce the expression of the hypoxia-inducible factor, HIF1- α , under normoxic conditions (Kim et al. 2007). Briefly, the WNT pathway stimulates the PI3K/Akt pathway and the transduction of WNT/ β -catenin target genes (such as c-Myc) to activate HIF-1 α activity in a hypoxia-independent manner (Kim et al. 2007). This, in turn, induces the expression of proteins involved in the promotion of aerobic glycolysis, such as glucose transporter, hexokinase 2, pyruvate kinase M2, pyruvate dehydrogenase kinase 1 and lactate dehydrogenase-A, leading to lactate production and activation of the Warburg effect (Kim et al. 2007). Moreover, Zhao et al. found that prostate CAF-derived exosomes could inhibit mitochondrial oxidative phosphorylation, thereby increasing glutamine-dependent reductive carboxylation and glycolysis in cancer cells (Zhao et al. 2016). Kunou et al. also showed that glycolysis and ATP production in lymphoma cells increased in the presence of CAF-released exosomes (Kunou et al. 2021). It has been shown that CD147 can upregulate expression of HIF-1 α and VEGF by PI3K/Akt pathway and play a key role as a chaperone to monocarboxylate transporters MCT1 and 4 (Zong et al. 2016). It is known that, due to the unmatched supply of oxygen, rapidly growing tumours rely largely on lactate oxidative metabolism for energy production and therefore CD147-MCT1/4 interaction seems to become the backbone for sustaining lactate and H⁺ trafficking and pH buffering (Le Floch et al. 2011). Our data showed that sEVs-CD147 induced Wnt/ β -catenin signalling pathway in recipient CAFs, thus stimulating the PI3K/Akt pathway and c-myc target gene expression that appears to be involved in the expression of aerobic glycolysis enzyme HK2, glucose and lactate transporter (SLC2A1 and SLC16A3, respectively). Moreover, we demonstrated that this phenomenon leads to an increased production of lactate, subsequently released in the extracellular milieu. Végan et al. showed that lactate stimulation causes an increase in the nuclear factor-kappa B (NF- κ B) pathway, which stops cell death by anti-apoptotic molecules and promotes cell survival. Qing et al. demonstrated that EVs stimulate the NF- κ B signalling pathway, activating fibroblasts to promote metastatic cancer cell growth by secreting proinflammatory cytokines (Végan et al. 2011; Ji

et al. 2020). We demonstrated that sEVs-CD147 can stimulate NF- κ B expression in CAFs, thus inducing the secretion of pro-inflammatory cytokines, such as IL-6 and IL-8. Lactate plays a major role in angiogenesis through VEGF stimulation (Ji et al. 2020). Several pieces of evidence suggest that NO promotes HIF-1 α stabilization, enhancing the effects of hypoxia in promoting tumour neoangiogenesis (Li et al. 2022; López-Sánchez et al. 2020). Our data showed that CR-CSC-released EVs induced VEGF expression and NO production in recipient CAFs, and these effects were associated with increased angiogenesis. All these effects were reverted or attenuated by blocking CD147 function on sEVs by specific antibody, N-deglycosylation or by the administration of AC73, a specific inhibitor of CD147. To evaluate if the effects are cell-line independent, we treated NFs with sEVs with different expression of CD147 and showed an increase of MCT4, VIM and NFK β expression in NFs, confirming that the observed effects are independent of the cell line used (data not shown). Moreover, using immunodeficient mice, we also demonstrated that CD147-enriched EVs derived from highly differentiated CRC-CSC accelerate cancer growth and that these effects were associated with metabolic reprogramming of CRC-CSC and CAF.

Spatial heterogeneity of cancer-cell clones as well as TME cellular components with diverse molecular characteristics and biological behaviour allow tumour cells to overcome microenvironmental constraints and modulate response to stress pressure such as cancer therapy (Seferbekova et al. 2023). For this reason, to gain a better understanding of the effects of sEVs-CD147 modulation, a spatial proteomics analysis was performed in mouse models following this experimental condition: CAF were cultured with sEVs derived from undifferentiated (sEVs low) or differentiated CRC-SCs (sEVs -CD147 high) or without EVs (vehicle/PBS) for 3 days. On Day 3, CRC-CSCs mixed with CAF treated with vehicle (PBS) or with sEVs (low and medium) were injected subcutaneously in the flank of NSG mice, and at Days 7, 14, and 21, mice were treated peritumorally with vehicle or sEVs. Adopting spatial proteomics analysis, we confirmed in vivo the activation of fibroblasts and the modulation of their metabolic features, within their biological context, after their conditioning with sEVs expressing different amounts of CD147. Our findings indicate that sEVs packaged CD147 activated CAF, and it is likely to speculate that this activation may contribute to tumour progression via stroma metabolism modification, although our experiment does not allow us to precisely quantify the effect of CAF activation on tumour growth. Moreover, we cannot conclude that the effect of sEVs -CD147 is limited to or stronger on CAF than on other TME cells. We have focused on CAFs in this study, but several pieces of evidence from our group and other authors suggest effects on other cell types as well (Nyalali et al. 2023; López-Sánchez et al. 2020; Zhao et al. 2016).

The horizontal spreading of oncogenic signals transferred by EVs after stress pressure (such as differentiating stimuli) may represent a mechanism of adaptation and resistance of tumour cells that, as they become less proliferative, can modulate the

TME (such as CAF or endothelial cells) to support the growth of specific, more resistant tumour clones. Overall, our findings indicate that sEVs-packaged CD147 activated CAFs and promoted tumour progression and angiogenesis. We have demonstrated these effects in both in vitro and in vivo models. However, the use of immunocompromised mouse models has some limitations: deficiency of T lymphocytes enables the engraftment and growth of the tumour cells in the subcutaneous xenograft, and the lack of a proper T lymphocytes immune response at the site of the primary tumour could not completely reflect the clinical scenario and warrants future investigation to confirm our findings. Another limitation of our study is that we did not definitively assess the role of sEV-induced CAF activation on tumour growth in vivo.

However, despite these limitations, our findings support an important role of EV-packaged CD147 in modulating and reprogramming TME metabolism and supporting tumour growth and warrant further studies to elucidate the mechanisms by which such effects are mediated.

Author Contributions

Donatella Lucchetti developed the original hypothesis, conceived the study, and designed experiments. Filomena Colella, Rita Colonna, Giulia Artemi, Sara Vitale, Giacomo Lazzarino, Federica Vincenzoni, and Sara Vitale performed the experiments. Donatella Lucchetti, Micol Eleonora Fiori, Giacomo Lazzarino analysed the data. Alessandro Sgambato and Donatella Lucchetti wrote and edited the manuscript. Ruggero De Maria edited the manuscript. Alessandro Sgambato supervised the study.

Conflicts of Interest

The authors declare no conflicts of interest.

Data Availability Statement

All data associated with this study are present in the article and the Supporting Information.

References

- Amorini, A. M., V. Nociti, A. Petzold, et al. 2014. "Serum Lactate as a Novel Potential Biomarker in Multiple Sclerosis." *Biochimica Et Biophysica Acta* 1842, no. 7: 1137–1143.
- Aoki, M., K. Koga, M. Miyazaki, et al. 2019. "CD73 complexes With emmprin to Regulate MMP-2 Production From Co-Cultured Sarcoma Cells and Fibroblasts." *BMC Cancer* 19, no. 1: 912. <https://doi.org/10.1186/s12885-019-6127-x>.
- Artiss, J. D., R. E. Karcher, K. T. Cavanagh, et al. 2000. "A Liquid-Stable Reagent for Lactic Acid Levels. Application to the Hitachi 911 and Beckman CX7." *American Journal of Clinical Pathology* 114, no. 1: 139–143.
- Bradford, M. M. 1976. "Rapid and Sensitive Method for the Quantitation of Microgram Quantities of Protein Utilizing the Principle of Protein–Dye Binding." *Analytical Biochemistry* 72, no. 1–2: 248–254. <https://doi.org/10.1006/abio.1976.9999>.
- Greaves, M., and C. C. Maley. 2012. "Clonal Evolution in Cancer." *Nature* 481, no. 7381: 306–313. <https://doi.org/10.1038/nature10762>.
- Ji, Q., L. Zhou, H. Sui, et al. 2020. "Primary Tumors Release ITGBL1-Rich Extracellular Vesicles to Promote Distal Metastatic Tumor Growth Through Fibroblast-Niche Formation." *Nature Communications* 11, no. 1: 1211. <https://doi.org/10.1038/s41467-020-14869-x>.

- Kalluri, R. 2016. "The Biology and Function of Fibroblasts in Cancer." *Nature Reviews Cancer* 16, no. 9: 582–598. <https://doi.org/10.1038/nrc.2016.73>.
- Kim, J. W., P. Gao, Y. C. Liu, G. L. Semenza, and C. V. Dang. 2007. "Hypoxia-Inducible Factor 1 and Dysregulated c-Myc Cooperatively Induce Vascular Endothelial Growth Factor and Metabolic Switches Hexokinase 2 and Pyruvate Dehydrogenase Kinase 1." *Molecular and Cellular Biology* 27, no. 21: 7381–7393. <https://doi.org/10.1128/MCB.00440-07>.
- Kunou, S., K. Shimada, M. Takai, et al. 2021. "Exosomes Secreted From Cancer-Associated Fibroblasts Elicit Anti-Pyrimidine Drug Resistance Through Modulation of Its Transporter in Malignant Lymphoma." *Oncogene* 40, no. 23: 3989–4003. <https://doi.org/10.1038/s41388-021-01829-y>.
- Lazzarino, G., A. M. Amorini, G. Fazzina, et al. 2003. "Single-Sample Preparation for Simultaneous Cellular Redox and Energy State Determination." *Analytical Biochemistry* 322: 51–59. <https://doi.org/10.1016/j.ab.2003.07.013>.
- Le Floch, R., J. Chiche, I. Marchiq, et al. 2011. "CD147 subunit of Lactate/H⁺ Symporters MCT1 and Hypoxia-Inducible MCT4 Is Critical for Energetics and Growth of Glycolytic Tumors." *Proceedings of the National Academy of Sciences* 108, no. 40: 16663–16668. <https://doi.org/10.1073/pnas.1106123108>. Epub September 19, 2011. Erratum in: *Proceedings of the National Academy of Sciences, USA*. December 4, 2012;109(49):20166.
- Naïken, Tanesha [corrected to Naiken, Tanesha]; Ilk, Karine [corrected to Ilc, Karine]. PMID: 21930917; PMCID: PMC3189052.
- Li, X., Y. Yang, B. Zhang, et al. 2022. "Lactate Metabolism in Human Health and Disease." *Signal Transduction and Targeted Therapy* 7, no. 1: 305. <https://doi.org/10.1038/s41392-022-01151-3>. Erratum in: *Signal Transduct Target Ther*. 2022 Oct 31;7(1):372. PMID: 36050306; PMCID: PMC9434547.
- Li, Z., C. Sun, and Z. Qin. 2021. "Metabolic Reprogramming of Cancer-Associated Fibroblasts and Its Effect on Cancer Cell Reprogramming." *Theranostics* 11, no. 17: 8322–8336. <https://doi.org/10.7150/thno.62378>.
- López-Sánchez, L. M., E. Aranda, and A. Rodríguez-Ariza. 2020. "Nitric Oxide and Tumor Metabolic Reprogramming." *Biochemical Pharmacology* 176: 113769. <https://doi.org/10.1016/j.bcp.2019.113769>.
- Lucchetti, D., F. Calapà, V. Palmieri, et al. 2017. "Differentiation Affects the Release of Exosomes From Colon Cancer Cells and Their Ability to Modulate the Behavior of Recipient Cells." *American Journal of Pathology* 187, no. 7: 1633–1647. <https://doi.org/10.1016/j.ajpath.2017.03.015>.
- Lucchetti, D., F. Colella, L. Perelli, et al. 2020. "CD147 Promotes Cell Small Extracellular Vesicles Release During Colon Cancer Stem Cells Differentiation and Triggers Cellular Changes in Recipient Cells." *Cancers* 12, no. 2: 260. <https://doi.org/10.3390/cancers12020260>.
- Lucchetti, D., C. Ricciardi Tenore, F. Colella, and A. Sgambato. 2020. "Extracellular Vesicles and Cancer: A Focus on Metabolism, Cytokines, and Immunity." *Cancers* 12, no. 1: 171. <https://doi.org/10.3390/cancers12010171>.
- Luo, Z., X. Dong, Q. Ke, Q. Duan, and L. Shen. 2014. "Downregulation of CD147 by Chitooligosaccharide Inhibits MMP-2 Expression and Suppresses the Metastatic Potential of Human Gastric Cancer." *Oncology Letters* 8, no. 1: 361–366. <https://doi.org/10.3892/ol.2014.2115>.
- Nyalali, A. M. K., A. U. Leonard, Y. Xu, et al. 2023. "CD147: An Integral and Potential Molecule to Abrogate Hallmarks of Cancer." *Frontiers in Oncology* 13: 1238051. <https://doi.org/10.3389/fonc.2023.1238051>.
- Patel, C. H., R. D. Leone, M. R. Horton, and J. D. Powell. 2019. "Targeting Metabolism to Regulate Immune Responses in Autoimmunity and Cancer." *Nature Reviews Drug Discovery* 18, no. 9: 669–688. <https://doi.org/10.1038/s41573-019-0032-5>.
- Seferbekova, Z., A. Lomakin, L. R. Yates, and M. Gerstung. 2023. "Spatial Biology of Cancer Evolution." *Nature Reviews Genetics* 24, no. 5: 295–313. <https://doi.org/10.1038/s41576-022-00553-x>.

- Shevchenko, A., H. Tomas, J. Havlis, et al. 2006. "In-Gel Digestion for Mass Spectrometric Characterization of Proteins and Proteomes." *Nature Protocols* 1: 2856.
- Sung, H., J. Ferlay, R. L. Siegel, et al. 2021. "Global Cancer Statistics 2020: GLOBOCAN Estimates of Incidence and Mortality Worldwide for 36 Cancers in 185 Countries." *CA: A Cancer Journal for Clinicians* 71, no. 3: 209–249. <https://doi.org/10.3322/caac.21660>.
- Taniguchi, K., and M. Karin. 2018. "NF- κ B, Inflammation, Immunity and Cancer: Coming of Age." *Nature Reviews Immunology* 18, no. 5: 309–324. <https://doi.org/10.1038/nri.2017.142>.
- Végran, F., R. Boidot, C. Michiels, P. Sonveaux, and O. Feron. 2011. "Lactate Influx Through the Endothelial Cell Monocarboxylate Transporter MCT1 Supports an NF- κ B/IL-8 Pathway That Drives Tumor Angiogenesis." *Cancer Research* 71, no. 7: 2550–2560. <https://doi.org/10.1158/0008-5472.CAN-10-2828>.
- Xu, J., Y. Lu, S. Qiu, Z. N. Chen, and Z. Fan. 2013. "A Novel Role of EMMPRIN/CD147 in Transformation of Quiescent Fibroblasts to Cancer-Associated Fibroblasts by Breast Cancer Cells." *Cancer Letters* 335, no. 2: 380–386. <https://doi.org/10.1016/j.canlet.2013.02.054>.
- Yakoub, K. M., G. Lazzarino, A. M. Amorini, et al. 2019. "Fructose-1,6-Bisphosphate Protects Hippocampal Rat Slices From NMDA Excitotoxicity." *International Journal of Molecular Sciences* 20, no. 9: 2239.
- Yan, W., X. Wu, W. Zhou, et al. 2018. "Cancer-Cell-Secreted Exosomal miR-105 Promotes Tumour Growth Through the MYC-Dependent Metabolic Reprogramming of Stromal Cells." *Nature Cell Biology* 20, no. 5: 597–609. <https://doi.org/10.1038/s41556-018-0083-6>.
- Zhao, H., L. Yang, J. Baddour, et al. 2016. "Tumor Microenvironment Derived Exosomes Pleiotropically Modulate Cancer Cell Metabolism." *Elife* 5: e10250. <https://doi.org/10.7554/eLife.10250>.
- Zong, J., Y. Li, D. Du, Y. Liu, and Y. Yin. 2016. "CD147 Induces Up-Regulation of Vascular Endothelial Growth Factor in U937-Derived Foam Cells Through PI3K/AKT Pathway." *Archives of Biochemistry and Biophysics* 609: 31–38. <https://doi.org/10.1016/j.abb.2016.09.001>. Epub Sep 9, 2016. Erratum in: *Archives of Biochemistry and Biophysics* Dec 15, 2016; 612:120. PMID: 27619643.

Supporting Information

Additional supporting information can be found online in the Supporting Information section.